Food Hydrocolloids 130 (2022) 107681

Contents lists available at ScienceDirect

Food Hydrocolloids

journal homepage: www.elsevier.com/locate/foodhyd

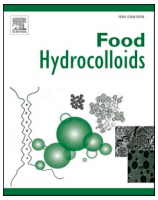

Instrumental characterization of xanthan gum and scleroglucan solutions: Comparison of rotational rheometry, capillary breakup extensional rheometry and soft-contact tribology

Xinxin Li [a,b], Stephen E. Harding [b], Bettina Wolf [c,**], Gleb E. Yakubov [a,*]

[a] Division of Food, Nutrition and Dietetics, School of Biosciences, University of Nottingham, Sutton Bonington Campus, Loughborough, LE12 5RD, UK
[b] National Centre for Macromolecular Hydrodynamics, University of Nottingham, Sutton Bonington Campus, University of Nottingham, Loughborough, LE12 5RD, UK
[c] School of Chemical Engineering, University of Birmingham, Birmingham, B15 2TT, UK

ARTICLE INFO

Keywords:
Xanthan gum
Scleroglucan
Rheology
Small amplitude oscillatory shear
Capillary break-up
First normal stress difference
Soft-contact tribology
Bovine submaxillary mucin
Saliva

ABSTRACT

Xanthan gum and scleroglucan, two rod-like polysaccharide hydrocolloids, are compared using a wide range of instrumental techniques and methods: steady shear flow, small amplitude oscillatory shear, first normal stress difference, capillary break-up and soft-contact tribology. The aqueous solutions of these two hydrocolloids with similar flow and viscoelastic profile show marked differences in capillary break-up time and apparent extensional viscosity. This result correlates with differences in first normal stress difference and, to a lesser extent, Stribeck curve behaviour. Formulating the hydrocolloids in concentrated sucrose solution (40 wt%) shifts relaxation profiles to longer times which greatly diminishes differences in rheological and lubrication behaviour. With exception of capillary break-up tests, no other methods showed statistically significant differences between the polysaccharides dissolved in the viscosified matrix. The toolbox of techniques is also applied to probe interactions of xanthan gum and scleroglucan with human whole saliva and bovine submaxillary mucin. We report no specific interactions between either hydrocolloid and salivary proteins and suggest that any cumulative effects must stem from specific sets of linear and non-linear rheological properties of saliva/hydrocolloid mixtures.

1. Introduction

Many food research and development tasks require making a choice of an instrumental technique for characterising flow and lubrication behaviour of food biopolymers and for exploring their interactions with other ingredients or biological interfaces. Combining different instrumental techniques presents a powerful approach that enables capturing different aspects of biopolymer behaviour at different length and time scales (Krop et al., 2020; Stokes et al., 2013; Stribiţcaia et al., 2020; Witt & Stokes, 2015). In the context of food product development, however, the combined approaches may present a number of practical challenges. Complexity of experimental design, difficulty of execution and data interpretation, as well as availability of instrumentation and considerable time investment may restrict wide adoption and impede practical utilisation. To address this problem and provide a simple comparison of instrumental techniques, we seek to examine the shear flow, viscoelastic and lubrication behaviour of two very similar hydrocolloid thickeners: xanthan gum and scleroglucan. We expect that different techniques would show selective sensitivity towards different facets of their viscoelastic behaviour. Further, in extension to our previous work using analytical ultracentrifugation (Li et al., 2020), we seek to utilise rheology and tribology tools to examine the interaction of these two hydrocolloids with salivary proteins.

The last decade saw significant progress in the development of experimental techniques for characterising food biopolymers and their behaviour during oral processing. Recent reviews by several research teams highlight the historical progression of food characterisation techniques (Boehm et al., 2019a, 2019b; Krop et al., 2019, 2020; Sarkar & Krop, 2019; Shewan, Stokes, & Smyth, 2020; Stokes et al., 2013; Stribiţcaia et al., 2020; Witt & Stokes, 2015) from approaches deeply rooted in flow profiling and rheological oscillatory techniques (small and large amplitude oscillatory shear rheometry (SAOS/LAOS)(Hyun et al., 2002; Stokes & Frith, 2008)) to advanced measurement capabilities. The next generation methods include thin gap high shear

* Corresponding author. ;
** Corresponding author.
E-mail addresses: B.Wolf@bham.ac.uk (B. Wolf), Gleb.Yakubov@nottingham.ac.uk (G.E. Yakubov).

https://doi.org/10.1016/j.foodhyd.2022.107681
Received 16 September 2021; Received in revised form 21 March 2022; Accepted 23 March 2022
Available online 6 April 2022

rheometry (Davies & Stokes, 2008), nanorheology using atomic force microscopy (Liamas et al., 2020; Vinogradova & Yakubov, 2006), extensional rheology approaches such as capillary break-up (Choi et al., 2014), as well as tribology and lubrication, with a particular focus on soft-contact tribology as one of the most effective technique for food-related applications (Pradal & Stokes, 2016; Sarkar et al., 2019a; Shewan, Pradal, & Stokes, 2020; Stribitcaia et al., 2020).

Although the choice of technique(s) is dictated by the research question(s), rheometer-based techniques are common go-to methods in many food development tasks that require evaluation of flow properties of thickeners and capturing the mouthfeel and texture properties of liquid and semi-liquid foods. However, many applications require evaluation of complex flow behaviours, as well as capturing the interactions of product ingredients and microstructures with saliva. These factors play a key role in determining oral processing of foods and have a profound impact on product's sensory attributes (Chen & Stokes, 2012; Sarkar et al., 2021; Sarkar & Krop, 2019). In the case of consumers who suffer from oropharyngeal dysphagia, saliva interactions with the product and complex flow behaviours, e.g. a simple spoonable or drinkable hydrocolloid formulation, need careful consideration in order to obtain a safe-to-eat product (Manrique et al., 2014, 2016; Newman et al., 2016). Two commonly employed formulation strategies for this kind of products include the use of rod-like high molecular weight thickeners such as xanthan gum, or weakly cross-linked systems such as carrageenan in which mineral salts are added to induce gelation (Newman et al., 2016; Qazi et al., 2017). The specific choice of a thickener system is dictated by rheological attributes (spooning, squeezing), texture properties and stability in different environmental conditions (ambient/chilled) and properties of the food/beverage matrix, i.e., pH, ionic strength, co-solutes.

Xanthan gum (XG) is a common choice in dysphagia formulations due to its unique shear-thinning properties (Song, Kim, & Chang, 2006) and low coil overlap concentration, c^* (Rodrigues et al., 2020), (ca. 0.01–0.03 wt% depending on the grade and the method of c^* determination). These properties stem from the rod-like conformation of XG chains as well as its weakly associative nature. To achieve the thickening effect, concentrations as low as 0.05 wt% XG may be sufficient to create an entangled, self-associated solution. This alleviates problems common in thickened foods such as diminished flavour and reduction in taste intensity (Baines and Morris, 1988, 1989; Preininger, 2016). Scleroglucan (SG) is a relatively less explored hydrocolloid, which, despite very different chemistry to XG, exhibits a markedly similar set of properties in solution. Similar to XG, SG has a rigid rod-like conformation and is largely non-charged (neutral), whereas XG is negatively charged. It is suggested that SG has a triple helix based structure (Lecacheux et al., 1986; Yanaki & Norisuye, 1983) which can further self-associate in a partially reversible way (Li et al., 2020). The shear thinning behaviour of XG and SG is one of the key flow properties that impacts oral processing. During bolus formation the force and shear fields play a key role, with the ingested food experiencing a mix of shear and elongational components of deformation (Stokes, 2012a). Further, rheological properties impact the way the oral surfaces come into rubbing contact during mastication. It should be noted that during oral processing of foods a rubbing contact forms at the interface between two oral surface, e.g. between the tongue and the hard palate, as well as between an oral surface, on one side, and the surface of a food particle or the surface of a semi-solid bolus, on the other. Within the rubbing contact, lubrication and friction become dominant properties, which can be explored using soft-contact tribology techniques, which utilise surfaces fabricated using compliant materials such as elastomers (Chen & Stokes, 2012; Stachowiak & Batchelor, 2013; Stokes, 2012b; Stokes et al., 2013; Yakubov, 2014).

Saliva is another key factor in oral processing and swallowing (Newman et al., 2016; Qazi et al., 2017). It has a marked and complex effect on the rheological properties of the bolus, depending on the nature of the food or beverage (Boehm et al., 2019b, 2020), as well as presence of starch which can be hydrolysed by salivary α-amylase during the oral processing stage (Humphrey & Williamson, 2001; Joubert et al., 2017; Pu et al., 2021). Enzymatic effects aside, saliva acts to hydrate solid particles and improve comminution of solid foods, whilst for beverages and thickened fluid-like formulations (e.g. yoghurts) it results in biopolymer dilution due to mixing (Boehm et al., 2020). The analysis of oral processing of beverages and soft solids is complicated by the fact that saliva in itself is a rheologically complex fluid (Stokes & Davies, 2007b), and hence the ratio of saliva to hydrocolloid solution will have a dramatic impact on the properties of mixtures (Yakubov et al., 2015). For example, saliva's bulk rheological properties are highly transient and change quickly after expectoration (Stokes & Davies, 2007b), whilst lubrication may display marked resilience towards processing conditions (Boehm et al., 2020). Although mimicking saliva is very challenging (Yakubov, 2014), it is possible to utilise mucin solutions as a proxy for probing fundamental mechanisms of hydrocolloid – mucin interaction that can guide development of hypotheses to be subsequently tested *ex/in vivo*. Another reason for using model salivary proteins is to circumvent inherent variability of saliva and mitigate the impact of its degradation upon collection (Sarkar et al., 2019b).

In this paper, we report comparative investigation of rheological and lubrication properties of two very similar rod-like polysaccharide thickeners: xanthan gum and scleroglucan. We use four different techniques: flow profiling using rotational rheometry (steady shear and first normal stress tests), small amplitude oscillatory shear rheometry, capillary break-up extensional rheometry and soft contact tribology. Further, we investigate the interaction of the polysaccharides with expectorated human whole saliva as well as a model mucin formulation, based on bovine submaxillary mucin and a cocktail of salts mimicking the ionic environment of human saliva (Sarkar & Krop, 2019). This is done to capture possible interactions of the biopolymer thickeners that may occur during oral processing which have important repercussions for food functionality and its sensory attributes, such as texture. Our results show that approaches based on a combination of techniques are very powerful, however, for similar viscoelastic biomolecules the capillary breakup extensional rheometry (CaBER) approach provides the most sensitive measure of subtle differences in viscoelastic behaviour and we suggest that this technique can be used as an effective proxy tool for evaluating viscoelastic properties of hydrocolloid solutions.

2. Materials and methods

2.1. Biopolymers and biopolymer solution preparation

Xanthan gum (Keltrol-T, CP Kelco, Surrey, UK) is used as received. Scleroglucan (Carbosynth, Compton, UK) is purified by centrifugation and dialysis. A 0.2% (w/v) turbid solution in water is centrifuged at 4850 g and 20 °C for 30 min. The supernatant is recovered by pouring out and then dialyzed in water to remove low molecular weight components. Then the dialyzed supernatant is freeze dried for 1 week in a freeze dryer (sample/condenser temperature are 16 °C and −55 °C, respectively) (Freeze Dryer Modulyo, Edwards, York, UK). The molecular properties of both the XG and the SG have been previously evaluated by a combination of sedimentation velocity and sedimentation equilibrium analytical ultracentrifugation, size exclusion chromatography coupled to multi-angle light scattering (SEC-MALS) and differential pressure viscometry and also capillary viscometry (Li et al., 2020). We also reported the (weight average) molecular weight of the XG and the SG as ~2880 kDa (Berth et al., 1996) and ~2800 kDa, respectively (Li et al., 2020).

Both biopolymer solutions are prepared in double-distilled water (18.2 MΩ cm). Sodium azide (Sigma-Aldrich, Gillingham, UK) is added as antimicrobial, 0.02% (w/v). To prepare the XG solution, sodium chloride (Sigma-Aldrich, Gillingham, UK) is added to stabilise the helical structure of the XG molecule (Abbaszadeh et al., 2016). The 1% (w/v) XG solution is prepared by slowly adding the appropriate amount

of XG into an aqueous solution of 0.2% (w/v) sodium chloride while mixing on a magnetic stirrer. Then, the solution is heated up to 80 °C, and stirred continuously at this temperature for 1 h. Finally, the solution is cooled down to room temperature (~20 °C) and left overnight before use. To prepare 0.2% (w/v) and 0.5% (w/v) XG solutions, the 1.0% (w/v) solution is diluted with the appropriate amount of aqueous solution of 0.2% (w/v) sodium chloride and mixed on a magnetic stirrer at 20 °C for at least 2 h.

The 1% (w/v) SG solution is prepared by slowly adding the appropriate amount of purified freeze-dried material into double-distilled water while mixing on a magnetic stirrer. To prepare more diluted SG solutions (0.2% (w/v) and 0.5% (w/v)), the 1% (w/v) solution is diluted with the appropriate amount of double-distilled water and mixed on a magnetic stirrer at 20 °C for at least 2 h.

Hydrocolloid solutions in sucrose are prepared by dispersing the appropriate amount of XG or SG in 40% (w/v) sucrose solution, slowly heating up to 80 °C and holding for 3 h under stirring conditions to obtain a fully dissolved material, as determined previously (Li et al., 2020). The 40% (w/v) sucrose solution is chosen as a solvent due to its higher viscosity compared to water while also showing Newtonian flow behaviour.

For the tribological experiments with the use of pre-adsorbed salivary films, 0.1% (w/v) biopolymer solutions (XG/SG) are prepared in PBS (phosphate buffered saline) buffer (pH = 6.8, I = 0.056 mol/L). The buffer is used to minimise changes of ionic environment upon contact with saliva (Macakova et al., 2010, 2011).

2.2. Saliva collection

Mechanically stimulated human whole saliva (HWS) is collected from one donor (female, 29 years old, non-smoking)(Carpenter et al., 2019; Fan et al., 2021). As saliva properties vary (Jehmlich et al., 2013), the saliva samples are always collected between 8.30 and 10.30 a.m., and the donor is requested to not eat or drink (with the exception of water) for at least 2 h before saliva collection. The donor also brushed their teeth after breakfast to remove as much food debris as possible. Prior to saliva collection, the donor rinsed the mouth with bottled water (Buxton natural mineral water) for at least 30 s to remove remaining food debris. Then, a 10 min rest period is imposed to allow the oral cavity to return to a neutral condition and to avoid dilution of donated saliva with water. For saliva collection, the donor is asked to chew on a small piece of laboratory film (Parafilm, Bermis Flexible Packaging, Neenah, USA) and expectorate the in-mouth collected volume of saliva every 30 s into a centrifuge tube. The total collection time is 6 min. The expectorated saliva from the first 30 s is discarded as it may contain food debris. During collection, saliva samples are kept on ice to minimise the saliva degradation. Then, the saliva samples are centrifuged at 10,000 g and 4 °C for 30 min, and the resulting supernatant collected. Immediately after supernatant collection, it is used to mix with the biopolymer solutions for further experiment.

2.3. Preparation of saliva mimic solution based on bovine submaxillary mucin

Saliva mimetic solution of bovine submaxillary mucin (BSM) (Sigma-Aldrich, Gillingham, UK), hereafter denoted reconstituted saliva (RS), is prepared using an aqueous solution of the composition detailed in Table 1 following the protocol described in Sarkar et al. (2009). These inorganic components and their concentrations are representative of HWS. The BSM is dissolved into this solution at the concentration of 30 mg/mL. This has comparable steady shear viscosity to that of HWS (Gal et al., 2001; Sarkar et al., 2009). A 0.12 mg/mL BSM solution is also prepared because this is the average concentration of mucin in human whole saliva (Kejriwal et al., 2014). However, addition of 0.12 mg/mL BSM solution to XG or SG solutions resulted in no effect on the capillary break-up behaviour (Table S1 and Table S2).

Table 1
Inorganic components in reconstituted saliva (Sarkar et al., 2009).

Component	Chemical formula	Concentration (g/L)
Sodium chloride	NaCl	1.594
Ammonium nitrate	NH_4NO_3	0.328
Potassium phosphate	KH_2PO_4	0.636
Potassium chloride	KCl	0.202
Potassium citrate	$K_3C_6H_5O_7.H_2O$	0.308
Uric acid sodium salt	$C_5H_3N_4O_3Na$	0.021
Urea	H_2NCONH_2	0.198
Lactic acid sodium salt	$C_3H_5O_3Na$	0.146

2.4. Biopolymer-saliva and reference mixture preparation

The centrifuged human whole saliva (HWS) supernatant and each biopolymer solution are separately mixed at a weight ratio of 1:5. The ratio was chosen based on the work by Choi et al. (2014), who considered the salivary flow rate with respect to the average volume of the fluid serving, of 10 mL. The concentrations of XG and SG solution used are both 0.5% (w/v). 0.5% of biopolymer solution is chosen for the extensional rheological analysis as 0.5% is the concentration of XG usually used in thickened food products (Choi et al., 2014). The mixing process took place in an ice water bath. For each saliva and biopolymer solution combination, six different stirring times are utilised in the capillary break-up test (2 min, 5 min, 30 min, 60 min, 90 min and 120 min). The control and BSM samples are prepared under the same condition, with the exception that the aliquot of saliva is replaced with double-distilled water or BSM solutions, respectively.

2.5. Steady shear and oscillatory shear rheological analysis

All of the shear rheological measurements are carried out at 20 °C by using a stress-controlled rheometer (MCR 301, Anton Paar, Graz, Austria) fitted with a cone-and-plate geometry (50 mm diameter, 2° cone angle). Each biopolymer solution is measured at least three times. For the steady shear rheological measurement, the shear rate ranges from 0.01 s^{-1} to 1000 s^{-1} and 10 logarithmically spaced data points are collected per decade. For the amplitude strain sweep test, the angular frequency is set at 1.59 Hz (10 rad/s) and the strain ranged from 0.01% to 1000%. For the frequency sweep test, the angular frequency ranges from 10 rad/s to 0.1 rad/s while the shear strain is set at 10%, which is within the linear-viscoelastic domain as shown by the results of the amplitude strain sweep tests.

2.6. Normal stress analysis

The normal stress measurements are also carried at a temperature of 20 °C using a stress-controlled rheometer (MCR 302, Anton Paar, Graz, Austria), fitted with a parallel plate geometry (50 mm diameter, 50 μm gap height) and applying gap error correction in accordance with published protocol by Davies and Stokes (2005). Triplicate analyses are carried out for each biopolymer solution. The first normal stress difference is measured in the shear rate range of 1000 s^{-1} to 10000 s^{-1} and parallel plate correction to the raw data is applied in accordance with the method described in Davies and Stokes (2008).

2.7. Filament break-up and data analysis

The extensional rheology tests are carried out at 20 °C using a capillary break-up extensional rheometer (CaBER-1, Thermofisher Haake, Karlsruhe, Germany). The operating principle of this method is based on the formation of a capillary bridge upon rapid separation of two cylindrical plates between which the test fluid is contained and monitoring the dynamics of the fluid column thinning (Mckinley & Sridhar, 2002). The thinning is followed by a laser micrometre at the midpoint of the filament length. For all measurements, 790 μL of sample

is placed between the fixed plate and the moving plate (diameter 6 mm). The initial gap is set at 3 mm. The strike time for the measurement is set at 20 ms and the final gap is set at 10 mm. Thus, the aspect ratio (AR = gap height between top and bottom plates/plate diameter) at the beginning of the test is 0.5 and at the end of the strike 1.67, corresponding to a Hencky strain of 1.2. Each sample is measured for at least 10 repeats, with a fresh aliquot being loaded for each replicate. Short values of the break-up time (<200 ms) render evaporation during experiments negligible. Data analysis is performed using Haake CaBER software.

The decay of the mid-point diameter (D) of a biopolymer solution has two regions, an exponential region and a linear region. In the linear region the impact of surface tension is much larger than the impact of gravity force, because the Bond number (Bo) is much smaller than 1 ($Bo = \left(\frac{L}{l_c}\right)^2 \approx 0.0016 \ll 1$, where L is the characteristic length ($L \sim D/2$–100 μm $= 10^{-4}$ m), $l_c \sim 2.5 \cdot 10^{-3}$ m is the capillary length) (Stelter et al., 2002, Mckinley, 2005). The biopolymer relaxation time (λ) and the steady state apparent extensional viscosity (η_e) are determined by fitting an initial exponential and a final linear region of the relationship of the midpoint dimeter versus time using Equations (1) and (2), respectively (Anna & Mckinley, 2001; Kheirandish et al., 2008; Stelter et al., 2002).

$$D(t) = D_0 \exp\left(-\frac{t}{3\lambda}\right) \tag{1}$$

$$\eta_e = -\frac{\sigma_s}{dD(t)/dt} \tag{2}$$

D is the diameter of the mid-point of the filament. D_0 is the mid-point diameter at time = 0. σ_s is the surface tension of the fluid. The surface tensions of XG and SG is 63.7 mN/m and 60.1 mN/m respectively, measured at 20 °C using a force tensiometer (Sigma 700, Biolin Scientific, Manchester, UK). When mixed with HWS, the surface tension of the XG-HWS mixture is 55.1 mN/m and that of the SG-HWS mixture 45.5 mN/m.

2.8. Stribeck tests

An MTM-2 mini traction machine is used to perform friction measurements (MTM-2, PCS Instruments Ltd., UK). The rubbing contact surfaces used here are a polydimethylsiloxane (PDMS) (SYLGARD® 184 Silicon Elastomer Kit, Dow Corning, MI) ball with the radius of 9.5 mm (diameter 19 mm) and a PDMS disk with the radius of 23 mm and the thickness of 4 mm. The Young's modulus of this PDMS material is 2.4 MPa (Bongaerts, Fourtouni, & Stokes, 2007). All PDMS surfaces involved in this research have a root mean square (r.m.s.) surface roughness of <10 nm. In a typical MTM experiment, the ball and the disc are driven independently at velocity v_{ball} and v_{disk} respectively, yielding the entrainment speed $U = (v_{ball} + v_{disk})/2$. The relative motion of the moving ball and the disc determine the slide-to-roll ratio, SRR = $|v_{ball} - v_{disk}|/U$. In all experiments, the SRR is set at 0.5 (50%). To prevent offset errors, lateral force measurements are taken at each entrainment speed when $v_{ball} > v_{disk}$ and $v_{ball} < v_{disk}$, both rotating in the same direction, and the average is taken. Further details on soft contact friction experiments are also presented elsewhere (Bongaerts, Fourtouni, & Stokes, 2007; Yakubov et al., 2009).

During the test, a load, L, is applied onto the ball and the normal force is measured using a strain gauge installed on the leaf spring of the MTM. In all experiments, L is set to 1 N. The lateral friction force, F_f, and the normal load yield the friction coefficient, $\mu = F_f/L$. One way of representing friction in different lubrication regimes is using a Stribeck curve, in which the friction coefficient is plotted against the product of U and the viscosity. For each entrainment speed, at a constant SRR, five friction measurements are taken and averaged (Bongaerts, Fourtouni, & Stokes, 2007). To test for hysteresis, each entrainment speed is tested twice in the same experiment; measurements are first taken from the highest speed of 1000 mm/s, decreasing step-wise to the lowest speed of 1 mm/s, after which the speed is increased again to 1000 mm/s. The tests are carried out with an inset to reduce the sample volume to 17 mL per run.

2.9. Friction measurement with the dynamic tribology protocol (DTP)

We also apply the Dynamic Tribology Protocol (DTP) in the MTM as this allows to probe the interaction of a salivary film with hydrocolloid solutions. DTP has been utilised before (Rossetti et al., 2009; Yakubov et al., 2015) and has recently received a thorough development by Fan et al. (Fan et al., 2021). During a typical DTP test, the friction coefficient at constant speed is recorded as a function of time. The measurement is started with saliva alone as a test fluid in order to pre-adsorb salivary proteins onto the hydrophobic PDMS surfaces which acts as the oral mimic (contact angle ca. 100°). At a specific time point, the hydrocolloid solution is added to the MTM chamber, and the temporal response of friction is recorded. Upon exposure of the salivary film to the hydrocolloid solution, the interaction changes the properties of the surface film resulting in changes in the friction coefficient. Typically, saliva is characterised by a very low friction coefficient (μ = 0.005–0.05) (Bongaerts, Rossetti, & Stokes, 2007), and the competitive binding of the hydrocolloid results in the loss of lubrication during the measurement.

The DTP curves of both biopolymers interacting with the pre-adsorbed salivary/mucin film are recorded using MTM-2 at the constant speed of 6 mm/s 0.1% (w/v) biopolymer solutions are used in these tests. 400 μl HWS (or saliva-mimetic BSM solution) is transferred by pipetting slowly on the disk in the first place to let the saliva form a thin film. The friction coefficient is recorded to monitor the formation process of the salivary film. Then 40 mL of 0.1% (w/v) XG or SG solutions (PBS buffer as the solvent) are poured into the chamber and the DTP temporal friction response is recorded with the rate of 1 reading/s. The DTP measurements are carried out at 35 °C, mimicking the temperature of the surfaces in the oral cavity.

3. Results and discussion

To illustrate our approach of using multiple techniques to probe and compare complex flow properties, we find it useful to provide a simple comparison of the rheological and lubrication data recorded using 0.5% (w/v) solutions of XG and SG. Fig. 1 presents a side-by-side comparison of the primary instrumental data (i.e., without further processing or analysis) obtained using the steady shear rheological test, oscillation tests, first normal stress difference test, capillary break-up test and Stribeck curve test. XG and SG exhibit similar steady shear flow behaviour and their viscoelastic responses within the linear viscoelastic range are found to be comparable. A marked difference is observed for the first normal stress difference. At shear rate 10^4 s^{-1}, the SG solution generates a two times larger normal force than that of XG. The filament break-up time of SG is also found to be two times higher than that of XG. Both normal force and filament break-up patterns indicate the effect of polymer chain stretching in shear and elongational flow, respectively. The friction coefficient of SG is found to be slightly higher than that of XG, clearly observed at low entrainment speeds, indicating potential differences in the behaviour of both hydrocolloids within a rubbing contact formed by two hydrophobic PDMS surfaces. The lubrication behaviour of SG at high entrainment speed (a transition from mixed to elasto-hydrodynamic lubrication) is marked by inlet starvation, as inferred from the shape of the Stribeck curve and the absence of a typical lubrication minimum. This minimum is clearly seen in the Stribeck curve for XG. This effect, we suggest, is associated with the observed viscoelastic behaviour, which, effectively, renders SG solutions to display a higher degree of rod climbing compared to XG, which disrupts fluid entrainment into the rubbing contact.

Based on examining results shown in Fig. 1, we made an observation

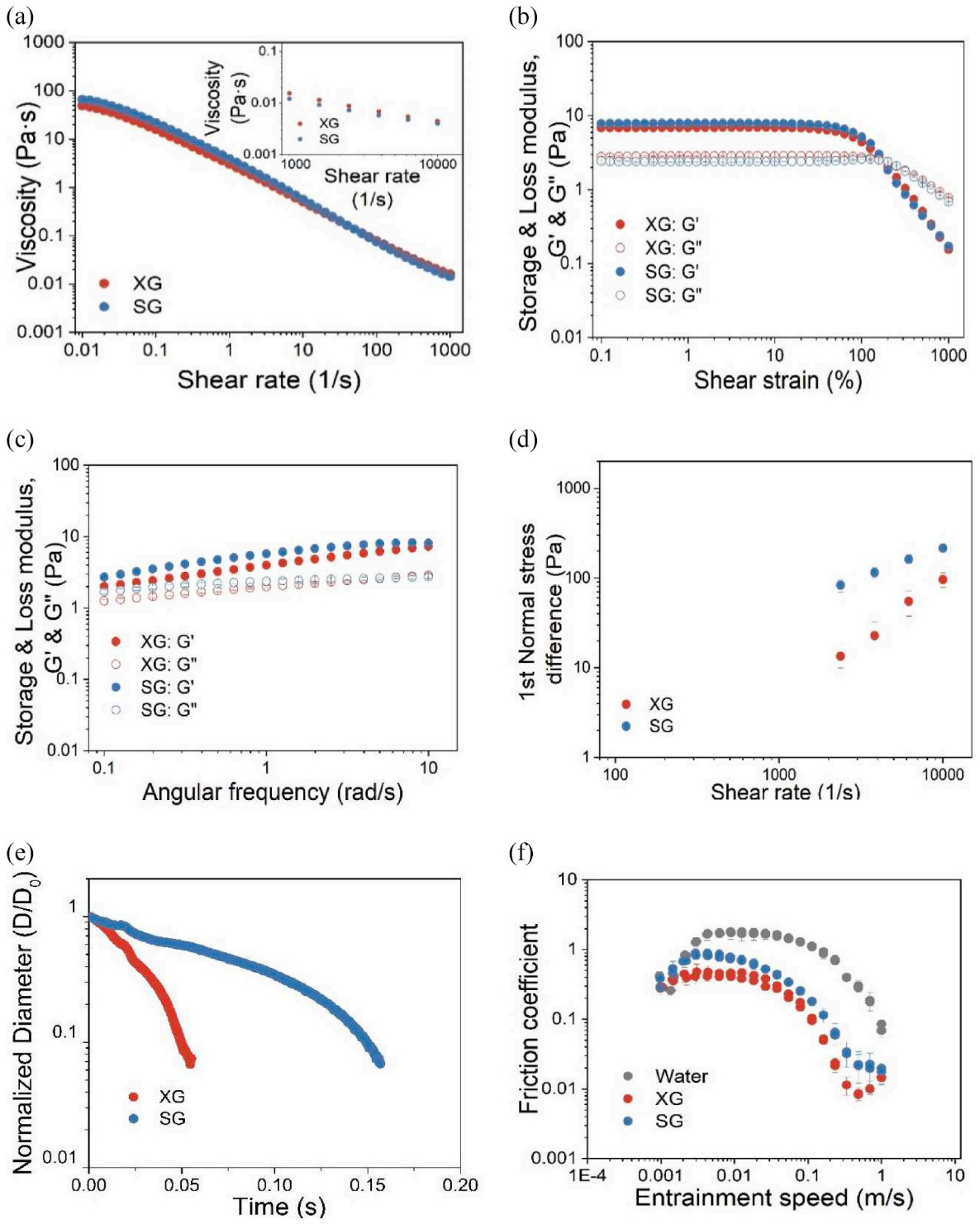

Fig. 1. Rheological and tribological data of 0.5% XG solution (red circles) and 0.5% SG solution (blue circles): (a) steady shear rheological tests (high shear section, 10^3 to 10^4 s^{-1}, is shown in the inset); (b) amplitude sweep test; (c) frequency sweep test recorded within the LVE range (oscillatory strain 10%); (d) first normal stress difference test; (e) filament break-up time; (f) Stribeck curve recorded at 1N load using hydrophobic PDMS tribopair (water contact angle ca. 100°, Young's modulus ca. 2.4 MPa). (For interpretation of the references to colour in this figure legend, the reader is referred to the Web version of this article.)

that extensional flow tests provide an easy-to-access method for discriminating differences in the viscoelastic behaviour between XG and SG. Following this observation, we examine each rheological/lubrication test in more detail and provide analysis of flow behaviour and its dependence on hydrocolloid concentration in order to shed light on the underlying mechanisms of polysaccharide chain relaxation. We also examine the effect of salivary proteins on the rheological and lubrication behaviour, with the view of scrutinising different methods with respect to their discriminating power.

3.1. Shear rheological analysis

The analysis of the rheological properties of XG and SG solutions at different concentrations is performed above the critical polymer coil

overlap concentration (c*) (Li et al., 2020; Cuvelier & Launay, 1986). Fig. 2 displays the steady shear flow behaviour of XG and SG solutions in the concentration range of 0.2%–1%. Both solutions have a comparable shear-thinning behaviour, although the viscosity of the SG solution is slightly higher than that of the XG solution at the low shear rate range of 0.01–1 s^{-1}. The viscosities of both solutions are moderately comparable in the shear range of 1–1000 s^{-1}. This is in good agreement with data reported by Lafforgue (Lafforgue et al., 2018). Some disagreement can be pointed out with data reported for SG by Moresi et al. (2001), reporting a 1% SG solution to be ~40 times more viscous than findings reported here. We associate this discrepancy with the purification method employed in this work (see Section 2.1), which results in removal of poorly soluble components. With regards to XG, our findings are in good agreement with many previous studies (see, for example, Phillips and Williams (2009)).

Fig. 3a shows the results of the small amplitude oscillatory shear tests. The viscoelastic moduli (amplitude sweep test) of the 0.2%, 0.5% and 1% XG and SG solutions each is found to be comparable, with both moduli increasing with concentration. Within the LVE range, the storage moduli are higher than the loss moduli for all concentrations tested for both, XG and SG solutions. At 0.2%, the damping factor ($\tan\delta = G''/G'$) of XG is higher than that of SG (Fig. 3b). With the increase of concentration, the difference of $\tan\delta$ between XG and SG becomes smaller. At the highest concentration (1%), the G'' of both biopolymer solutions displays an overshoot phenomenon at the cross-over point (also known as the flow point), i.e., where $G' = G''$. In accordance with Donley et al. (2020), this phenomenon is the manifestation of the transition from solid-like, viscoelastic dissipation to fluid-like, plastic flow at larger amplitudes, whereby strain within the overshoot region is associated with fluid-like (viscoplastic) deformation, as opposite to the LVE range where strain is dominated by solid-like (viscoelastic) deformation. Due to the universal nature of this yielding mechanism, our findings appear to be consistent with previous research on hydrocolloid systems (Hyun et al., 2002; Lafforgue et al., 2018; Ren et al., 2020; Song, Kuk, & Chang, 2006).

The frequency sweep test shows a typical viscoelastic behaviour with both moduli increasing with concentration (Fig. 3c). The SG solutions show higher storage and loss moduli compared to the XG solutions of the same concentration. The 0.5% and 1% solutions exhibit elasticity dominated ($G' > G''$) viscoelastic behaviour within the frequency range tested (0.1–10 rad/s). For the 0.2% XG and SG solutions, the cross-over point is observed at 2 rad/s and 6 rad/s for XG and SG, respectively. Accordingly, tan δ of XG is somewhat higher than that of SG at the same concentration, and the differences become bigger with increasing angular frequency (Fig. 3d). Further, for both, XG and SG solutions, the Cox-Merz plot (Cox & Merz, 1958) reveals that the complex viscosity is slightly higher than the steady shear viscosity (Supplementary Fig. S1). Lopes da Silva et al. (1993) suggested that this phenomenon can be caused by high associations between molecules or the presence of an entangled network (Augusto et al., 2013).

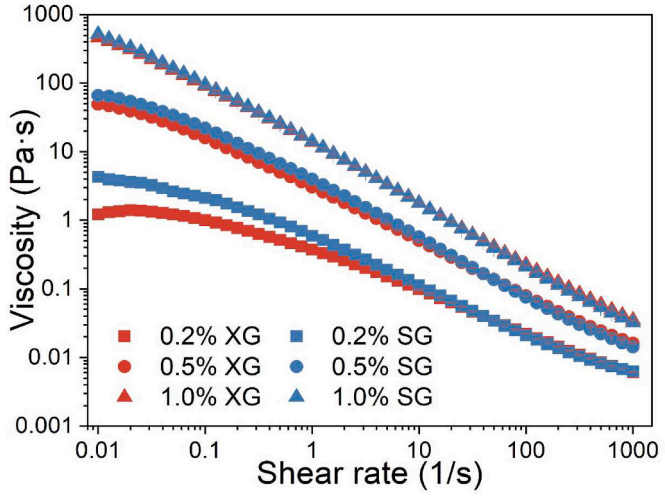

Fig. 2. Shear rheological properties of XG (red symbols) and SG (blue symbols) solution in water at 20 °C and varying concentrations: 0.2% (square), 0.5% (circle) and 1% (triangle). The error bars are within the size of the symbol. (For interpretation of the references to colour in this figure legend, the reader is referred to the Web version of this article.)

3.2. Normal stress analysis and extensional behaviour

To probe viscoelastic behaviour further, the normal stress difference profiles are measured using narrow gap parallel plate rheometry (Davies & Stokes, 2008). The normal stress (i.e., the component of the stress tensor orthogonal to the shear plane) can be viewed as a measure of polymer resistance to stretching in response to the shear force (Song, Kim, & Chang, 2006), which in turn alters the streamlines of the flow generating stress components in the direction perpendicular to the shear plane. Fig. 4a shows the 1st normal stress difference data of 0.5% XG and 0.5% SG. For relatively dilute biopolymer solutions, the normal forces are relatively weak. However, N_1 increases with the shear rate, enabling detection at higher values of $\dot{\gamma}$. For experiments in water, as shown in Fig. 4a, the practical range of shear rates with detectable normal force is found between 10^3 to 10^4 s^{-1}. SG shows higher N_1 values compared to XG, and, consequently, SG is characterised by the higher values of the 1st normal stress coefficient Ψ_1 (described in Eq. (3)) (Larson, 1999).

$$N_1 = \sigma_{xx} - \sigma_{yy} = \Psi_1 \cdot \dot{\gamma}^2 \tag{3}$$

σ_{xx} and σ_{yy} are the stress components in the direction parallel and perpendicular to the direction of the rheometer's plate, respectively. For polymer solutions and melts and for conditions where $\dot{\gamma}\to 0$, $\Psi_{1,0}$, is proportional to the shear viscosity with coefficients depending on the specific details of the model used, i.e., a model of a polymer solution or a melt. The simplest expression takes the form (Larson, 1999):

$$\Psi_{1,0} = 2\eta_p \tau_D = 2(\eta - \eta_s)\tau_D \tag{4}$$

η_p is the polymer component of viscosity, i.e., solution viscosity (η) is represented as the superposition of the polymer component and the solvent viscosity (η_s), $\eta = \eta_p + \eta_s$. τ_D is the characteristic relaxation time, typically taken as the longest relaxation time (Larson, 1999). For higher shear rates ($\dot{\gamma}\to\infty$), the expression for $\Psi_{1,\infty}$ is more complex, as it depends on the finite extensibility of the polymer chains (e.g., finitely extensible nonlinear elastic model, FENE). Although precise analysis relies on computational solutions, for rod-like polymers the asymptotic relation takes the following form (Stewart & Sorensen, 1972):

$$\Psi_{1,\infty} = 2\eta_p \tau_D \frac{1}{(\tau_D \dot{\gamma})^{4/3}} \tag{5}$$

Using the expression for the viscosity of a polymer solution expressed as a product of the modulus (Gp) and the characteristic relaxation time (Doi & Edwards, 1986), $\eta_p \approx \eta_{p_a} = G_{p_a}\tau_{D_a}$, we obtain a simplified relation of these parameters to the 1st normal stress coefficient (Eq. (6)). In the expression above, the superscript a denotes the apparent nature of the quantities, reflecting the fact that the system is away from zero-shear conditions.

$$\Psi_{1_a,\infty} = 2G_{p_a}\tau_{D_a}^2 \frac{1}{(\tau_{D_a}\dot{\gamma})^{4/3}} \tag{6}$$

In order to disentangle the contributions of G_p and τ_D, we use 40% sucrose solution as a viscosified Newtonian solvent. Firstly, the shear stress in a viscosified solvent is higher for a given value of $\dot{\gamma}$, which makes the practical implementation of first normal force measurements more robust, i.e., the values of the measured normal force are well above instrument sensitivity. Secondly, under conditions of higher stress a

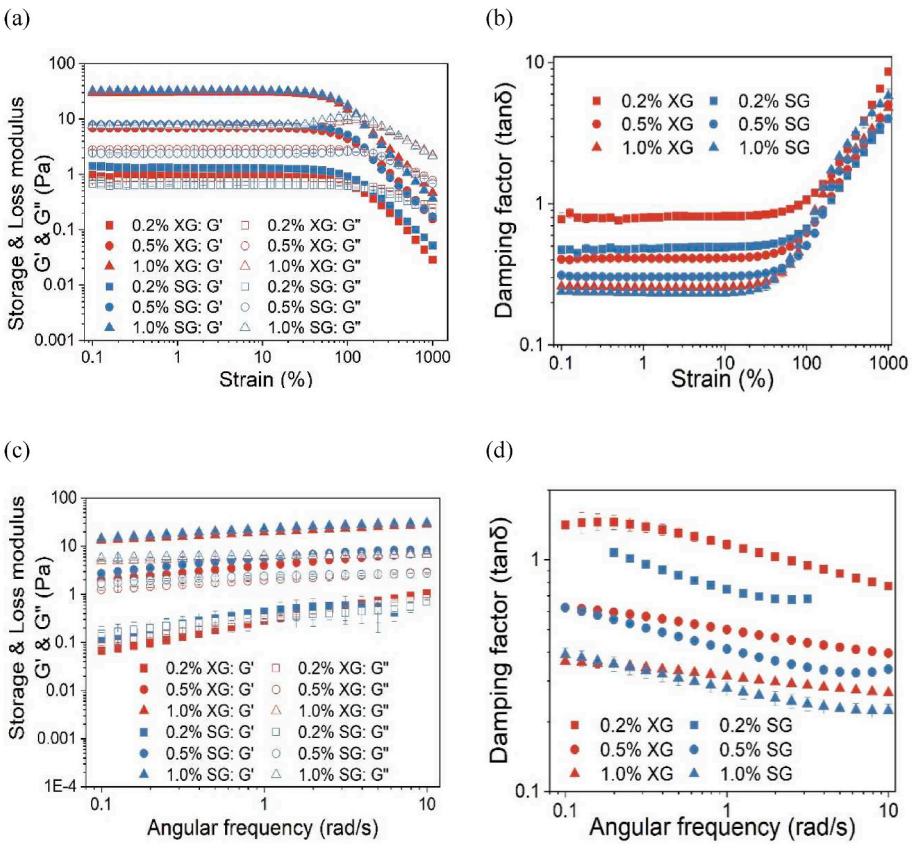

Fig. 3. Oscillatory shear profiles of XG (red symbols) and SG (blue symbols) solutions with the concentration of 0.2% (squares), 0.5% (circles) and 1% (triangles) at 20 °C. Amplitude sweep test: storage modulus (filled symbols) and loss modulus (open symbols) (a), and damping factor (tanδ) (b). Frequency sweep test: storage modulus (filled symbols) and loss modulus (open symbols) (c), and damping factor (tanδ) (d). (For interpretation of the references to colour in this figure legend, the reader is referred to the Web version of this article.)

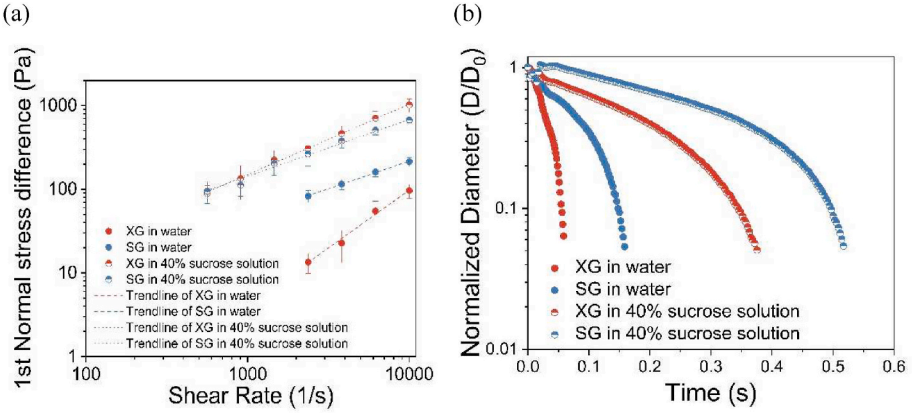

Fig. 4. (a) First normal stress difference of XG solution and SG solution at 20 °C in water and 40% sucrose. In water, the trendline of XG is $y = 0.00028x^{1.39}$, the trendline of SG is $y = 0.50x^{0.66}$ In 40% sucrose, the trendline of XG is $y = 0.45x^{0.84}$, the trendline of SG is $y = 1.2x^{0.69}$. (b) The normalized filament diameter of 0.5% XG (red symbol)s and 0.5% SG solution (blue symbols) in water (filled symbols) and 40% sucrose solution (half-filled symbols) as a function of time. (For interpretation of the references to colour in this figure legend, the reader is referred to the Web version of this article.)

polymer molecule extends more giving rise to slower relaxation modes.

As expected (Zirnsak et al., 1999), the values of N_1 are higher than in aqueous solutions of XG and SG, however, the difference between two biopolymers reduces to below experimental error. These results suggest that XG and SG have comparable G_p and τ_D, and therefore differences observed in water are likely to be associated with the complex relaxation spectrum and shorter relaxation modes of the polymer chain. If the latter would be the factor, the difference in N_1 between XG and SG would remain regardless of solvent viscosity or, equivalently, regardless of characteristic elongation time. Further analysis of the dependency of N_1 on $\dot{\gamma}$ shows that for SG, the scaling exponent is very close to the theoretical prediction of 2/3 (for water and 40% sucrose solution), suggesting short and long relaxation processes correspond to fundamentally the same relaxation structure. By contrast, the scaling parameter for XG in water is ~3/2, suggesting dilute-like behaviour (i.e., away from the stretching limit of the polymer chain, $N_1 \sim \dot{\gamma}^2$). In 40% sucrose solution, it reduces to ~0.8, which comes somewhat nearer to the value of 2/3 predicted for the rigid rod structure in accordance with a dumbbell FENE (or FENE-P) model (Bird et al., 1987; Doi & Edwards, 1986). The observed differences in the viscoelastic response may point to the structural differences of XG in water and 40% sucrose. It is possible to propose a potential mechanism rooted in the weak self-association of XG. In that scenario, XG single chains dominate the viscoelastic response at short relaxation times, whilst the rod-like double-stranded assemblies dominate the viscoelastic response at longer relaxation times. These findings are consistent with the values of the power exponent for XG, varying from 0.09 to 1.47, reported across different concentrations and solvents (Escudier et al., 1999; Stokes et al., 2001; Wei et al., 2014; Zirnsak et al., 1999).

Following the result from the normal stress analysis we examine the

dependency of the decay of the normalized filament diameter of 0.5% XG and SG solutions in water and 40% sucrose solution (Fig. 4b). The results show that both, XG and SG solutions have two regimes, i.e., an exponential regime and a linear regime. This is also validated by previous researchers (Stelter et al., 2002, Mckinley, 2005). The relaxation time can be calculated from the exponential region of the filament break-up curve using Eq. (1). If the solution's surface tension is known, the steady state extensional viscosity can be calculated from the linear region of the filament break-up curve using Eq. (2).

Table 2 summarises the calculated values of the filament break-up time, relaxation time, steady state extensional viscosity of XG/SG in water/40% sucrose solution. Although the values of the filament break-up time can vary with different final gap and different strike time settings, our measurements of the filament break-up time of XG and SG solutions are found to be consisted with several previous studies (see for example (Turcanu et al., 2015; Sousa et al., 2011, Japper-Jaafar et al., 2009)). The filament break-up time, the relaxation time, and the steady state extensional viscosity of SG solutions in water are two times higher than the corresponding values of the XG solutions. This result is consistent with the lower values of the 1st normal stress difference of XG as compared to the SG. In 40% sucrose solution, the difference between the two hydrocolloids diminishes, which again is consistent with the results of the normal force evaluations (Fig. 4). We also note that the values of the extensional viscosity are similar, which is consistent with the results from steady shear and SAOS analysis.

To summarise, the rheological data indicate that XG and SG have a very similar hydrodynamic volume (Li et al., 2020), but their chain dynamics appears rather different. Taking the normal force and extensional data together, it is possible to suggest that faster relaxation modes in XG may contribute to the faster filament breakup. In addition, the stability of supra-molecular association can play a significant role. These data are consistent with previous AUC results suggesting that SG assemblies may be more stable compared to those formed in solution by XG (Li et al., 2020).

3.3. Concentration dependence of the stribeck behaviour of XG and SG

Based on the rheological characterisation, we establish that XG and SG have comparable shear rheological behaviour and linear viscoelasticity. However, they display different non-linear viscoelasticity. Here we explore the tribological behaviour of XG and SG under different concentrations by utilising a Stribeck curve formalism. A Stribeck curve is one of the most effective ways to present the friction behaviour of a thin fluid film under different conditions of fluid entrainment between solid surfaces (Stachowiak & Batchelor, 2013). The Stribeck curve can be generated by plotting the coefficient of friction on the y axis versus the product of entrainment speed (U) and fluid viscosity (η) divided by the load (L) applied on the upper surface, $\eta U/L$, on the x axis. The unit of $\eta U/L$ is m^{-1}. In this work, however, the load applied on the upper ball is constant and set at 1 N; this allows us to simplify the Stribeck plot and use reduced velocity, defined as ηU (N/m), as the x axis (Fig. 5) (Selway et al., 2017).

Table 2
Filament break-up time, relaxation time, steady state extensional viscosity of XG and SG in water/40% sucrose solution.

	Filament break-up time (ms)	Relaxation time (ms)	Steady state apparent extensional viscosity (Pa·s)
XG in water	59.0	11.1	28.9
XG in 40% sucrose solution	376.0	81.3	168.0
SG in water	167.0	27.7	52.3
SG in 40% sucrose solution	519.0	127.6	192.2

In the most general case, a Stribeck curve has three regimes: boundary regime, mixed regime and elasto-hydrodynamic regime (Chen & Stokes, 2012; Stokes, 2012b; Yakubov, 2014). When the entrainment speed is low, the asperities on the surfaces can lock and lead to high values of the friction coefficient (boundary regime). When the entrainment speed is high, the fluid film between surfaces can give the upper surface a lift force, and the friction coefficient is the smallest. However, with the increase of the entrainment speed, the drag force caused by the surface movement increases faster than the lift force. The friction coefficient will increase again, known as the elasto-hydrodynamic regime. Between the boundary and elasto-hydrodynamic regimes, there is a mixed regime, where fluid film becomes discontinuous and the proportion of the PDMS-PDMS asperity contacts increases. The minimal friction coefficient is at the turning point of the mixed regime and the elasto-hydrodynamic regime (De Vicente, Spikes, & Stokes, 2006). Parameters such as the viscosity of the fluid, the mechanical and surface properties of the rubbing solids, i.e., roughness and contact angle, control the lubrication behaviour of fluid film (Bongaerts, Fourtouni, & Stokes, 2007; Selway et al., 2017; Stokes, 2012b; Xu & Stokes, 2020).

Constructing a Stribeck curve for non-Newtonian fluids is more complex, because the value of the product, $\eta(\dot{\gamma} = f(U))\cdot U$, is affected by the shear rate dependent viscosity of the fluid. In Fig. 5a and b respectively, we present experimental results considering low shear (0.01 s^{-1}) viscosity, denoted $\eta_{0.01}$, and high shear (1000 s^{-1}) viscosity, denoted η_{1000}. In Fig. 5b, the Stribeck curves for water are shown for the reference and to highlight the difference of boundary friction behaviour between pure water and the hydrocolloid solutions. The viscosity data can be found in Supplementary Table S5. Since the viscosity of XG and SG is comparable at the same concentration (Fig. 2 and Supplementary Table S5), the Stribeck curves of both biopolymer solutions formulated at the same concentration appear in a similar position with respect to the x axis.

The Stribeck behaviour of the XG solutions is in good agreement with several previous publications (see for example (Chojnicka-Paszun & De Jongh, 2014; Stokes et al., 2011, de Vicente et al., 2005)). The friction behaviour of SG has previously been studied by Garrec and Norton (2012), and our friction coefficient data compare well with their data. In the boundary regime, the SG solution shows a higher friction coefficient than the XG solution at all concentrations tested. The dependency of the coefficient of friction on concentration is weak, suggesting that in the range of concentrations tested we do not observe complex (e.g., multi-layer) adsorption of the polymer onto the PDMS surface. We also note that for both solutions a nonparallel boundary region is observed, which is caused by the unstable measurement on a smooth PDMS surface at low entrainment speed (Selway et al., 2017; Xu & Stokes, 2020).

In the mixed regime and choosing low shear viscosity to scale the Stribeck curves (Fig. 5a), the curves do not quite overlap with the horizonal shift decreasing with decreasing difference in the low shear viscosity. When scaling with the high shear viscosity though, as can be seen from Fig. 5b, most of the data in the mixed regime overlap. Since the high shear viscosity can be assumed to be much more representative of the viscosity in the gap between the friction partners, due to the narrow gap and the magnitude of the entrainment speeds, the tribological data acquired on the XG and SG solutions suggest that the viscosity is the dominant factor in this regime in the tribological contact (Stokes, 2012b).

Within the range of entrainment speeds applied, the elasto-hydrodynamic regime is only observed for the 1% solutions, both for XG and SG, as the drag force on the upper surface from the fluid is apparently not strong enough at the lower solution concentrations applied.

The first normal stress difference tests showed that when XG and SG are dissolved in 40% sucrose solution, they have comparable non-linear viscoelasticity. It is, therefore, hypothesized that XG and SG in 40% sucrose solution behave similar in tribological tests. Fig. 6 shows

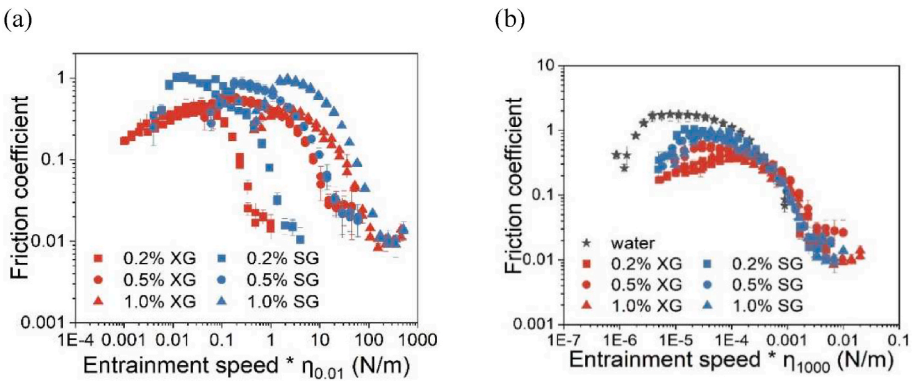

Fig. 5. Stribeck curves of XG solutions (red symbols) and SG (blue symbols) solution (water as the solvent) with the concentrations of 0.2%, 0.5% and 1% at 20 °C: (a) friction coefficient vs entrainment speed·$\eta_{0.01}$, (b) friction coefficient vs entrainment speed·η_{1000}. The data for water (star symbols) are given for comparison. One can see that all curves align in the mixed regime, but display different boundary friction at the low values of $U\eta$. (For interpretation of the references to colour in this figure legend, the reader is referred to the Web version of this article.)

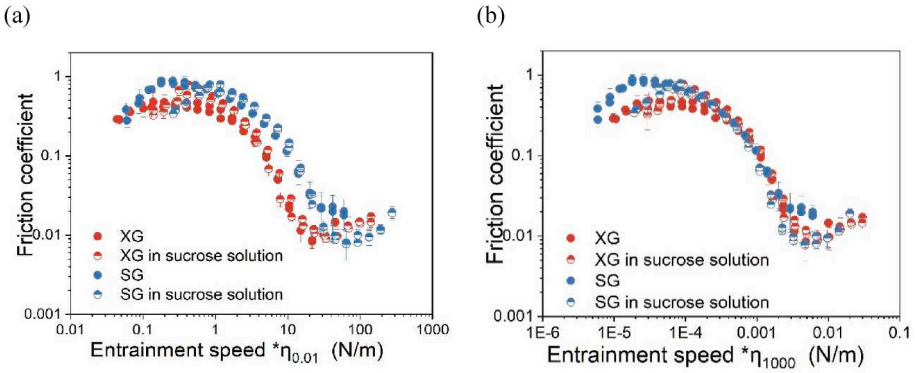

Fig. 6. Comparison of Stribeck curves of 0.5% XG (red symbols) and 0.5% SG solutions (blue symbols) in water (filled symbols) or in 40% sucrose (half-filled symbols) at 20 °C: friction coefficient vs entrainment speed·$\eta_{0.01}$ (a), friction coefficient vs entrainment speed·η_{1000} (b). (For interpretation of the references to colour in this figure legend, the reader is referred to the Web version of this article.)

Stribeck curves, plotted equivalent to the curves in Fig. 5, for XG and SG dissolved in water and in 40% sucrose solution (viscosity data are reported in Supplementary Table S5). Thanks to the higher viscosity of 40% sucrose solution, the elasto-hydrodynamic regime is extended, and the boundary regime is shortened, allowing probing the entire Stribeck curve for both hydrocolloids. The friction coefficient of XG in the boundary regime is found to be higher in 40% sucrose solution than in water, suggesting that the presence of sucrose may affect XG interaction with PDMS. By contrast, the friction coefficient of SG in the boundary regime is essentially unaffected by the solvent.

In the mixed regime, the friction coefficient of SG and XG in 40% sucrose solution and in water collapse onto a single curve, when η_{1000} is used as the scaling factor. This result suggests that high-shear viscosity is the dominant parameter in the mixed and elasto-hydrodynamic regimes, which is consistent with previous results of N_1 and extensional rheological measurement. The $U\eta_{1000}$ values at the friction minimum can be used to provide estimations of the thickness of the lubricating film in the soft-elastohydrodynamic contact based on the approximate expressions obtained by de Vicente, Stokes and Spikes (de Vicente et al., 2005). For the solutions in 40% sucrose, we obtain the value for the minimum film thickness of ~3 μm and the central thickness of ~5.8 μm (the details of the model are provided in the Supplementary Information).

3.4. Rheological analysis of mixing biopolymer solutions with HWS and RS

In our previous work (Li et al., 2020), using analytical ultracentrifugation (AUC), we found no evidence for interactions between XG or SG and bovine submaxillary mucin (BSM) dissolved in a saliva-mimicking buffer (RS). This result may indicate that both polysaccharides are inert with respect to BSM or else the binding constant is low. The latter means that in the dilute system the equilibrium is pushed away from the formation of complexes. In this work, we examine the mechanism of complex formation (or absence thereof) using more concentrated biopolymer solutions (10 times higher concentrations) which shifts the equilibrium towards formation of complexes (Rodrigues et al., 2021). We also take advantage of good solubility of XG and SG in viscosified 40% aqueous sucrose to probe interactions in the solvent system with lower water activity (a_w ~ 0.95). We hypothesise that use of 40% sucrose may promote polysaccharide-protein or polysaccharide-mucin interactions due to lower 'availability' of water molecules. In addition, we analyse the behaviour of mixtures of XG and SG with human whole saliva (HWS). Saliva is a multi-component biological fluid, which, in addition to mucin, is comprised of several other classes of (glyco)proteins (Yakubov et al., 2014). The interaction of non-mucin salivary proteins with XG or SG may also affect saliva rheology and lubrication and, hence, comparison between purified mucin and whole saliva provides a more detailed analysis of possible scenarios that may unravel during the oral processing of XG/SG-containing foods. In these experiments, we too use water and 40% sucrose as solvents to probe the effect of small molecule weight solutes on biopolymer interactions.

Analysis of steady shear and small amplitude oscillatory shear profiles show no evidence that adding mucin or saliva to a biopolymer solutions has any influence on flow properties or LVE behaviour in water and 40% sucrose (Supplementary Figs. S2 and S3). This result appears to be consistent with previous findings by Choi et al. (2014), suggesting that the interaction between XG and SG with mucin or other salivary proteins is very weak.

To boost measurement sensitivity, we employ the extensional CaBER technique to probe the impact of RS (BSM) and HWS on the behaviour of polysaccharides under conditions of large elongational strains. We propose that under these conditions even weak interactions may

influence the behaviour of polysaccharides in the extensional flow by interfering with the mechanism of polymer chain relaxation. Fig. 7 shows the decay of the normalized filament diameter of 0.5% XG and SG solutions and their mixtures with RS/HWS.

Table 3 summarises the results of the evaluation of the filament break-up time, the relaxation time and the steady state extensional viscosity of the biopolymer solutions (0.5%) mixed with water (control samples), HWS or RS. For the mixing conditions, the stirring time of 5 min is used; this value is chosen to ensure that saliva deterioration has a consistent impact on all samples.

Surprisingly, we find that mixtures or biopolymer solutions with HWS or RS show a markedly longer break-up time compared to the pure polysaccharide solutions. This results is particularly striking because the estimated values of the extensional viscosity for the mixtures are lower or identical to that of the pure polysaccharides (Table 3). This result is also counterintuitive in another aspect: the absolute solid content of the mixtures is actually higher due to the presence of additional biopolymers in the form of mucin and salivary proteins. Consequently, the solutions would be expected to have a higher viscosity, whilst the experimental results show the opposite. Given the values of extensional viscosity for the mixtures are lower, the increase in the values of the break-up time must be underpinned by the longer relaxation times. This conclusion is supported by the analysis of the exponential region of the filament break-up curve, results of which are shown in Table 3 and summarised in Supplementary Tables S1 and S2. For XG, the presence of RS or HWS results in an increase of the relaxation time by ~42% or ~28%, respectively. For SG, the increase is smaller and ~17–19% for both, RS and HWS.

The extensional flow behaviour in the presence of RS or HWS is scrutinised further by a) examining the same mixtures dissolved in 40% sucrose and b) replacing the rod-like hydrocolloids with the coil-like dextran. For the latter case, we build on the previous research by Choi et al. (2014), who reported an increase of the filament break-up time of carboxymethyl cellulose (CMC)-HWS mixtures. CMC has a much lower molecular weight (ca. 200–300 kDa), making it harder to draw comparisons with XG or SG (Mw ca. 2800 kDa). Therefore, dextran (T2000, Mw ca. 2000 kDa) is chosen for these experiments. To match the filament break-up time of XG, 20 wt% solution of T2000 dextran in water is used.

Like aqueous counterparts, SG solutions in 40% sucrose show a higher filament break-up time, relaxation time and steady state extensional viscosity compared to XG. When hydrocolloids are mixed with HWS or RS, the filament break-up time is ~25% and ~13% larger for SG and XG, respectively. Although the trend in 40% sucrose appears to be reversed compared to water, the results show a high degree of consistency between both solvents. The behavior of dextran solutions echoes the results obtained for XG and SG (Table S4), with the increase of the filament break time due to the presence of RS or HWS being much larger. For RS the measured increase is ca. 65%, whilst for HWS it is ca. 90–95%. Some preliminary results using other proteins indicate that the effect of the increase in capillary break-up time may be a generic property of polysaccharide-protein systems under conditions of extensional flow (Borah & Yakubov, 2021).

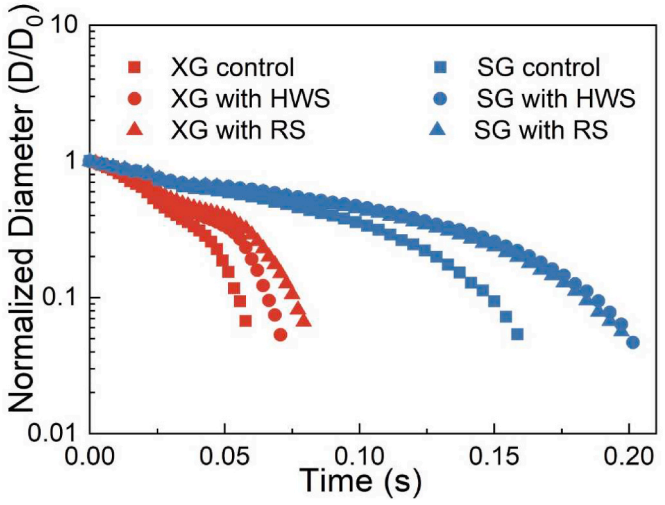

Fig. 7. The normalized filament diameter of 0.5% XG (red symbols) and 0.5% SG solution (blue symbols) mixed with water (squares), HWS (circles) or RS (triangles) as a function of time with the mixing stirring time under 2 min at 20 °C (water as the solvent). (For interpretation of the references to colour in this figure legend, the reader is referred to the Web version of this article.)

Table 3
The filament break-up time, relaxation time and steady state extensional viscosity of control, HWS samples and RS samples of XG and SG solutions in water. Stirring time is 5 min.

	Filament break-up time (ms)	Relaxation time (ms)	Steady state apparent extensional viscosity (Pa·s)
XG control	60.4 ± 1	11.1 ± 0.4	25.1 ± 1.8
XG with HWS	70.6 ± 1.7	14 ± 0.5	19.7 ± 0.8
XG with RS	78.3 ± 2.3	15.6 ± 0.1	24.0 ± 0.8
SG control	159.2 ± 5.1	27 ± 3.5	56.9 ± 2.6
SG with HWS	190.1 ± 3.4	30.8 ± 1.2	50.2 ± 1.3
SG with RS	203.3 ± 7	31.1 ± 1.7	53.1 ± 2.5

Although our findings require further examination and testing, we can propose that weak interactions between salivary proteins and polysaccharide hydrocolloids may occur during the extensional deformation of polysaccharides. It is possible to hypothesise that in the extended state, where conformation flexibility is restricted, the reduction in chain entropy may be compensated by the condensation of salivary proteins (or mucins) onto the extended polysaccharide chain, which delays chain retardation from the extended state back into a coil. Addressing this hypothesis would require future research and probing the detailed structure and molecular alignment during liquid bridge formation. That said, the proposed hypothesis appears to be consistent with the results obtained in 40% sucrose versus water, where XG chains relax fast and salivary proteins elicit a stronger effect on the break-up time. Conversely, in 40% sucrose the polysaccharide chains relax slower and hence the 'boost' from salivary proteins is, comparatively, smaller.

From a method development perspective, we also explore the effect of stirring time on the filament break-up time, relaxation time and steady state extensional viscosity. Fig. 8 summarises the results obtained using 0.5% hydrocolloids mixed with water (control samples), HWS and RS under different stirring time. The effects of time and saliva 'aging' are well-documented (Punyadeera et al., 2010; Stokes & Davies, 2007a); it is hypothesized that stirring time will reveal the effect of saliva proteolytic degradation and its impact on extensional rheology of XG and SG solutions (in water). It is anticipated that RS will show higher stability, thus offering additional flexibility and robustness of the analysis if practical uses of these tests are in mind. The results show that changes upon 'aging'/stirring time are relatively small, which may indicate that the saliva degradation effects are offset by the dilution effect, or else the degradation occurs within first 2 min of mixing, with further mixing time having little effect. Albeit the magnitude of the observed changes being small, the results of the ANOVA tests summarised in Supplementary Table S3 clearly show that for the mixtures of XG/SG with HWS the reduction in filament break-up time with the increase of stirring time is systematic and statistically significant (P values < 0.05). As expected, RS shows higher stability compared to HWS, and the observed changes with

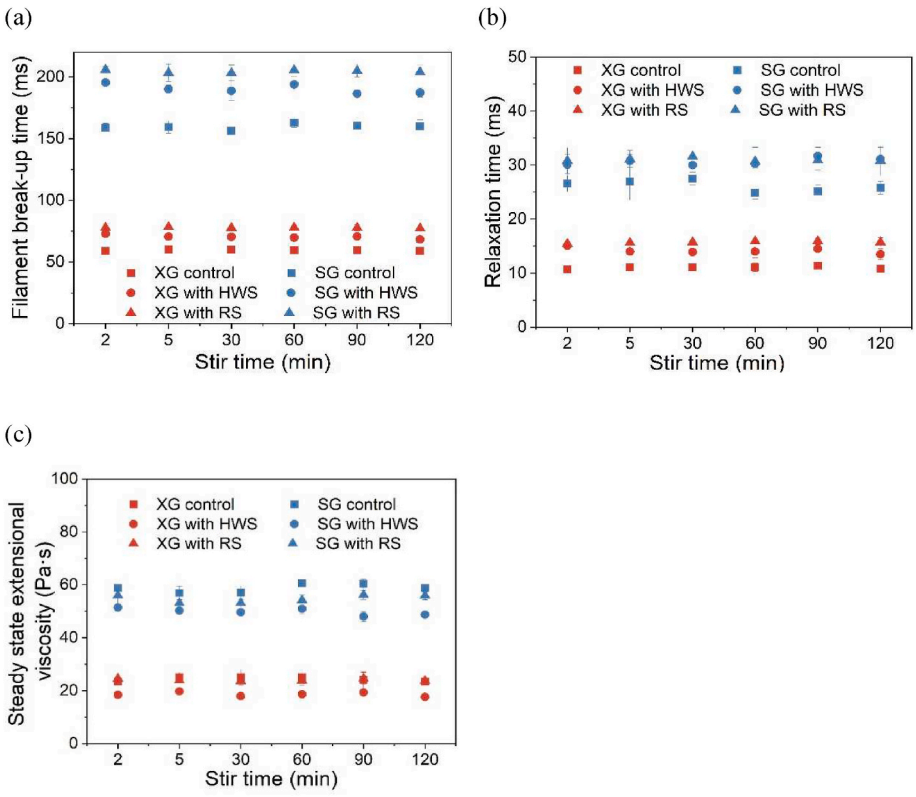

Fig. 8. Effect of stirring time on (a) filament break-up time, (b) relaxation time, and (c) steady state extensional viscosity of control (squares), HWS samples (circles) and RS samples (triangles) of 0.5% XG (red symbols) and 0.5% SG solution (blue symbols). (For interpretation of the references to colour in this figure legend, the reader is referred to the Web version of this article.)

stirring time are found to be within the experimental error. (The same trends for HWS and RS, respectively, are observed for 20 wt% T2000 dextran solutions mixed with HWS, see Supplementary Table S4 for the reference).

3.5. *Tribological analysis of mixing biopolymer solutions with HWS or RS*

In the absence of strong interactions between XG/SG and HWS/RS, the tribological properties of the mixtures will be governed by the relative propensity of biopolymers to adsorb onto the hydrophobic PDMS surface. The competition between hydrocolloid and proteins will determine the composition of the adsorbed layer, which, in turn, will control the lubrication and friction behaviour of the mixtures. It is envisaged that these insights will shed some light on the behaviour of XG/SG-based formulations during oral processing. Although the use of soft contact tribology technique cannot replicate full complexity of the human mouth, it enables probing some fundamental interactions between rod-like hydrocolloids and salivary films. The data generated in this work will be instrumental for uncovering possible mechanisms underpinning functional properties and sensory attributes of XG/SG-based dysphagia formulations. Together with rheological measurements, soft-contact tribology provides a new set of tools for understanding complex processes such as such as oral lubrication, swallowing, and texture.

In this work, we utilise two soft-contact tribology methodologies: a) Stribeck curve analysis (De Vicente, Stokes, & Spikes, 2006) and a simplified variant of the dynamic tribology protocol (DTP) (Fan et al., 2021). The first method aims to explore lubrication behaviour of the mixtures in the wide range of entrainment speeds, whilst the latter aims to understand the ability of hydrocolloid to displace a pre-adsorbed salivary film. The presence of the adsorbed salivary/mucin film on PDMS is well-established, and it has been shown to be the leading mechanism for the observed reduction in friction (Macakova et al., 2010; Yakubov et al., 2009). It is expected that mucin will reduce friction to <0.2, and for saliva the coefficient of friction may be as low as 0.01 (Bongaerts, Rossetti, & Stokes, 2007) (the typical range is between 0.01 and 0.1 depending on the donor and collection method). The presence of hydrocolloids is expected to interfere with the adsorption process, leading to the changes in the coefficient of friction. We note, that in Section 3.3 it has been established those pure hydrocolloids are not as lubricious as saliva or mucin, and hence we expect that in the presence of XG/SG the friction will increase. Although the direct measurements of adsorption (e.g. using QCM-D and/or ellipsometry (Macakova et al., 2011; Pradal et al., 2019; Rodrigues et al., 2021) have not been employed in this work, the friction data led us to firm conclusions, forming a strong basis for the future exploration.

3.5.1. *Effect of addition of RS or HWS on stribeck behaviour*

Fig. 9 shows the Stribeck curves of the polysaccharide solutions in water and 40% sucrose mixed with HWS or RS. The Stribeck curves are constructed using η_{1000} as the scaling factor (See Section 3.3 and Fig. 5). The values of viscosity at 1000 s^{-1} are provided in Supplementary Table S5.

In the mixed and elasto-hydrodynamic regimes all Stribeck curves overlap. This is due to the comparable values of shear viscosity and similarity of the shear-thinning behaviour of XG and SG and their mixtures with HWS or RS. For solutions in 40% sucrose (Fig. 9b), it is possible to surmise that the overlap in the elasto-hydrodynamic regime is less precise compared to when η at 0.01 s^{-1} is used as the scaling factor (see Supplementary Fig. S5). Possible explanation of this discrepancy could be associated with errors in determining the viscosity at 1000 s^{-1} in sucrose solutions, where the stresses are higher compared with the solutions in water.

In the boundary regime, the friction coefficients of the XG-HWS and

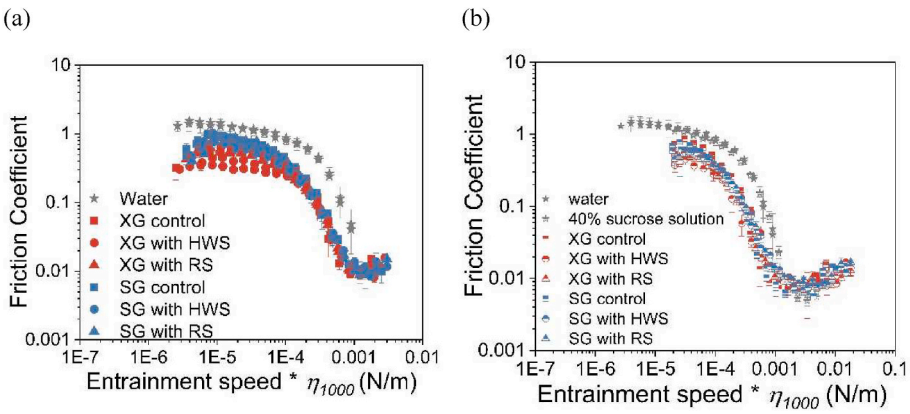

Fig. 9. Stribeck curves of XG (red symbols) and SG solution (blue symbols) mixed with water (squares), HWS (circles) or RS (triangles) at 20 °C: (a) water as the continuous phase (filled symbols), (b) 40% sucrose solution as the continuous phase (half-filled symbols). The Stribeck curves for water (filled stars) and 40% sucrose (half-filled stars) are provided for comparison. (For interpretation of the references to colour in this figure legend, the reader is referred to the Web version of this article.)

XG-RS mixtures are lower than the controls, and this difference is more apparent for XG-HWS than for XG-RS (Fig. 9a). On the contrary, HWS or RS have little influence on the friction coefficient of the SG solutions in the boundary regime. This result suggests that SG dominates the friction response as evident from the comparison between Stribeck curves recorded in SG solution and pure water (or 40% sucrose). The coefficient of friction between PDMS surfaces in water (or 40% sucrose) is ca. 1.3 times higher (at $U = 6$ mm/s) than in SG solution, suggesting that SG modulates PDMS surface and renders it more lubricious, albeit marginally. This conclusion is also true for XG, but, under conditions of this experiment, the propensity of XG to dominate the friction response in the presence of salivary proteins is weaker. This points to the lower adsorption strength of XG on PDMS surfaces (De Vicente, Stokes, & Spikes, 2006; Stokes et al., 2011).

3.5.2. *Evaluation of XG and SG using the dynamic tribology protocol (DTP)*

The analysis of the mixed solutions indicates that the hydrocolloids dominate the friction response of the mixtures. This however does not consider the effect of dilution on the formation of a HWS or RS film on PDMS. Using the DTP, we first form an adsorbed layer of HWS or RS on PDMS (Fan et al., 2021) and then we introduce the hydrocolloid solution to monitor the modification of the pre-adsorbed film by XG or SG.

To perform this test, 400 μl HWS or RS are slowly transferred to the disk rotating at low speed (6 mm/s) to form a thin layer of HWS or RS. The friction coefficient data recorded during this time period correspond to pure HWS or RS. In Fig. 10, these data are shown using filled symbols. Throughout this stage, the friction coefficient of HWS and RS are comparable, both range from 0.03 to 0.12, which is comparable with data reported previously (Bongaerts, Rossetti, & Stokes, 2007; Macakova et al., 2010, 2011; Madsen et al., 2014).

In the second stage, 40 mL of XG or SG solutions are poured into the chamber of the MTM machine, and the friction coefficients are recorded (shown as open symbols in Fig. 10). In this test, the hydrocolloids are dissolved in PBS buffer to ensure that the pH and ionic strength of HWS or RS is not changed abruptly. It is found that the friction coefficients of the hydrocolloid-HWS systems remains unchanged upon addition of hydrocolloids, suggesting that HWS forms a stable film, lubricating properties of which is not affected by hydrocolloids. For the hydrocolloid-RS systems, the friction coefficient increases immediately after addition of the hydrocolloid solutions. The SG-RS mixture has a higher fiction coefficient than the XG-RS mixture, which is consistent with the fact that pure SG has higher friction coefficient as compared to XG (see Fig. 5 for reference).

A simplified analysis of the dependence of the friction coefficient on time is performed using first order kinetics approximation. The use of this simple model rests on the assumption that the friction coefficient is proportional to the concentration of the material on the surface. It is assumed that upon the addition of the hydrocolloid, it either displaces mucin from the surfaces or it forms a complex at the interface, and said complex has lower lubricity. The analysis using the first order kinetics model is shown in Fig. 10b. We find that the effective binding constant of hydrocolloids is somewhat higher for SG ($k = 0.0103 \pm 0.0003$) than for XG ($k = 0.0076 \pm 0.0003$), which is consistent with our inference from the analysis of the Stribeck curves that SG has stronger adsorption than XG. It should be noted that both hydrocolloids do not exhibit a strong lubricating effect, i.e., the friction coefficients are not too dissimilar to those of pure water and at least an order of magnitude higher than for HWS. Although such behaviour may be undesirable for hydrocolloids used in dry mouth formulations, the water-like friction coefficient is consistent with their functionality as texturizing agents.

When comparing the results of the hydrocolloid-RS with the hydrocolloid-HWS systems, it is evident that the pre-adsorbed film

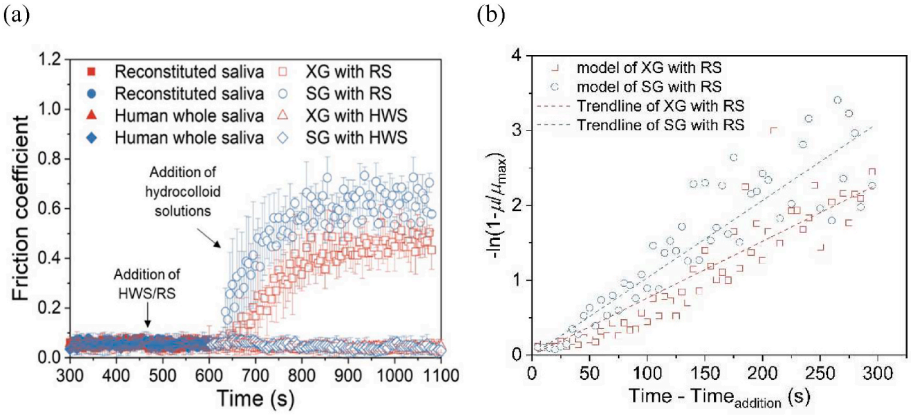

Fig. 10. Comparison of steady state values of the coefficient of friction for XG and SG solutions deposited on pre-adsorbed BSM and HWS surface films at 35 °C: (a) open symbols indicate the HWS or RS film (solely), the corresponding filled symbols indicate the friction coefficient after pouring biopolymer solutions, (b) The analysis of the dependence of friction coefficient on time for XG and SG with RS. The friction data are plotted in the linearized form to yield effective binding constants.

formed by RS is different to that formed by HWS. This result is in good agreement with several previous studies which established that mucin cannot mimic the lubrication properties of saliva (see for example (Kesimer & Sheehan, 2008; Raynal et al., 2002; Sarkar et al., 2019c; Veeregowda et al., 2012; Yakubov et al., 2014; Yakubov et al., 2015).

The 1st order kinetic analysis indicates that SG has a higher binging constant which is consistent with the Stribeck tests that show SG lubrication is not affected by the presence of salivary proteins. At the same time, SG's ability to facilitate lubrication is weak. We suggest that SG's ability to adsorb to PDMS is governed by its neutral charge, which facilitates hydrophobic interaction with PDMS. At the same time, the absence of charges results in no electrostatic repulsion that keeps surfaces apart and prevents the formation of high friction asperity contacts. By contrast, XG is negatively charged, which contributes to some disjoining pressure within the confined liquid film. However, weak adsorption makes such barrier susceptible to shear and rubbing forces, rendering XG to be an inefficient lubricant.

4. Concluding remarks

In this research, we demonstrate that SG and XG display comparable shear rheological and linear viscoelastic behaviours. However, they possess different non-linear viscoelasticity and tribological properties. In order to probe the non-linear domain of the viscoelastic behaviour we utilise the capillary break-up test and normal force difference measurement. The break-up test appears to be markedly more sensitive, and easier to execute.

Our findings suggest that XG and XG have a similar hydrodynamic volume, but their mechanism of polymer chain relaxation is different. We propose that XG features relaxation modes that in comparison with SG are faster. This results in the lower values of the normal force and shorter filament break-up times. We highlight the utility of using viscosified solvent (such as 40% sucrose) as a tool to modify the relaxation spectrum of polysaccharide hydrocolloids.

We also document that SG and XG have weak interaction with saliva, and that SG has a stronger propensity to adsorb on hydrophobic surfaces compared to XG.

In practice, these insights and the development of the methodological toolbox provides new opportunities to select as well as 'mix-and-match' different methods to probe complex flow and friction behaviour, which has strong potential to facilitate the development of new and improved food formulations using rod-like polysaccharide hydrocolloids.

Credit author statement

Xinxin Li: Conceptualization, Methodology, Investigation, Analysis, Writing - original draft. **Stephen E. Harding**: Funding acquisition, Resources, Supervision, Writing – reviewing & editing. **Bettina Wolf**: Conceptualization, Funding acquisition, Resources, Supervision, Writing – reviewing & editing. **Gleb E. Yakubov**: Conceptualization, Funding acquisition, Resources, Supervision, Methodology, Analysis, Writing – reviewing & editing.

Declaration of competing interest

There are no conflicts of interest.

Acknowledgements

X.L. acknowledges financial support through a Vice Chancellor's Scholarship from the University of Nottingham. G.E.Y. acknowledges the financial support from the Biotechnology and Biological Sciences Research Council (BBSRC) grant (BB/T006404/1).

Appendix A. Supplementary data

Supplementary data to this article can be found online at https://doi.org/10.1016/j.foodhyd.2022.107681.

References

Abbaszadeh, A., Macnaughtan, W., Sworn, G., & Foster, T. J. (2016). New insights into xanthan synergistic interactions with konjac glucomannan: A novel interaction mechanism proposal. *Carbohydrate Polymers, 144*, 168–177.
Anna, S. L., & Mckinley, G. H. (2001). Elasto-capillary thinning and breakup of model elastic liquids. *Journal of Rheology, 45*, 115–138.
Augusto, P. E. D., Falguera, V., Cristianini, M., & Ibarz, A. (2013). Viscoelastic properties of tomato juice: Applicability of the cox–merz rule. *Food and Bioprocess Technology, 6*, 839–843.
Baines, Z., & Morris, E. (1988). Effect of polysaccharide thickeners on organoleptic attributes. *Gums and stabilisers for the food industry*, 193–201.
Baines, Z., & Morris, E. (1989). Suppression of perceived flavour and taste by food hydrocolloids. *Food colloids, 75*, 184–192.
Berth, G., Dautzenberg, H., Christensen, B. E., Harding, S. E., Rother, G., & Smidsrød, O. (1996). Static light scattering studies on xanthan in aqueous solutions. *Macromolecules, 29*, 3491–3498.
Bird, R. B., Curtiss, C. F., Armstrong, R. C., & Hassager, O. (1987). *Dynamics of polymeric liquids* (Vol. 2). New York: John Wiley & Sons, Inc. Kinetic Theory.
Boehm, M. W., Warren, F. J., Baier, S. K., Gidley, M. J., & Stokes, J. R. (2019). A method for developing structure-rheology relationships in comminuted plant-based food and non-ideal soft particle suspensions. *Food Hydrocolloids, 96*, 475–480.
Boehm, M. W., Yakubov, G. E., Delwiche, J. F., Stokes, J. R., & Baier, S. K. (2019). Enabling the rational design of low-fat snack foods: Insights from in vitro oral processing. *Journal of Agricultural and Food Chemistry, 67*, 8725–8734.
Boehm, M. W., Yakubov, G. E., Stokes, J. R., & Baier, S. K. (2020). The role of saliva in oral processing: Reconsidering the breakdown path paradigm. *Journal of Texture Studies, 51*, 67–77.
Bongaerts, J. H. H., Fourtouni, K., & Stokes, J. R. (2007a). Soft-tribology: Lubrication in a compliant PDMS–PDMS contact. *Tribology International, 40*, 1531–1542.
Bongaerts, J. H. H., Rossetti, D., & Stokes, J. R. (2007). The lubricating properties of human whole. *Saliva, 27*, 277–287.
Borah, P., & Yakubov, G. E. (2021). In T. U. O. Nottingham (Ed.), *Unpublished data of okra polysaccharide-protein systems*.
Carpenter, G., Bozorgi, S., Vladescu, S., Forte, A. E., Myant, C., Potineni, R. V., Reddyhoff, T., & Baier, S. K. (2019). A study of saliva lubrication using a compliant oral mimic. *Food Hydrocolloids, 92*, 10–18.
Chen, J., & Stokes, J. R. (2012). Rheology and tribology: Two distinctive regimes of food texture sensation. *Trends in Food Science & Technology, 25*, 4–12.
Choi, H., Mitchell, J. R., Gaddipati, S. R., Hill, S. E., & Wolf, B. (2014). Shear rheology and filament stretching behaviour of xanthan gum and carboxymethyl cellulose solution in presence of saliva. *Food Hydrocolloids, 40*, 71–75.
Chojnicka-Paszun, A., & De Jongh, H. H. J. (2014). Friction properties of oral surface analogs and their interaction with polysaccharide/MCC particle dispersions. *Food Research International, 62*, 1020–1028.
Cox, W. P., & Merz, E. H. (1958). Correlation of dynamic and steady flow viscosities. *Journal of Polymer Science, 28*, 619–622.
Cuvelier, G., & Launay, B. (1986). Concentration regimes in xanthan gum solutions deduced from flow and viscoelastic properties. *Carbohydrate Polymers, 6*, 321–333.
Davies, G. A., & Stokes, J. R. (2005). On the gap error in parallel plate rheometry that arises from the presence of air when zeroing the gap. *Journal of Rheology, 49*, 919–922.
Davies, G. A., & Stokes, J. R. (2008). Thin film and high shear rheology of multiphase complex fluids. *Journal of Non-newtonian Fluid Mechanics, 148*, 73–87.
De Vicente, J., Spikes, H. A., & Stokes, J. R. (2006). Viscosity ratio effect in the emulsion lubrication of soft EHL contact. *Journal of Tribology, 128*, 795–800.
De Vicente, J., Stokes, J. R., & Spikes, H. A. (2005a). The frictional properties of Newtonian fluids in rolling–sliding soft-EHL contact. *Tribology Letters, 20*, 273–286.
De Vicente, J., Stokes, J. R., & spikes, H. A. (2005b). Lubrication properties of non-adsorbing polymer solutions in soft elastohydrodynamic (EHD) contacts. *Tribology International, 38*, 515–526.
De Vicente, J., Stokes, J. R., & Spikes, H. A. (2006). Soft lubrication of model hydrocolloids. *Food Hydrocolloids, 20*, 483–491.
Doi, M., & Edwards, S. F. (1986). *The theory of polymer dynamics*. Oxford: Oxford University Press.
Donley, G. J., Singh, P. K., Shetty, A., & Rogers, S. A. (2020). Elucidating the G″ overshoot in soft materials with a yield transition via a time-resolved experimental strain decomposition. *Proceedings of the National Academy of Sciences, 117*, 21945.
Escudier, M. P., Presti, F., & Smith, S. (1999). Drag reduction in the turbulent pipe flow of polymers. *Journal of Non-newtonian Fluid Mechanics, 81*, 197–213.
Fan, N., Shewan, H. M., Smyth, H. E., Yakubov, G. E., & Stokes, J. R. (2021). Dynamic Tribology Protocol (DTP): Response of salivary pellicle to dairy protein interactions validated against sensory perception. *Food Hydrocolloids, 113*, 106478.
Gal, J.-Y., Fovet, Y., & Adib-Yadzi, M. (2001). About a synthetic saliva for in vitro studies. *Talanta, 53*, 1103–1115.
Garrec, D. A., & Norton, I. T. (2012). The influence of hydrocolloid hydrodynamics on lubrication. *Food Hydrocolloids, 26*, 389–397.
Humphrey, S. P., & Williamson, R. T. (2001). A review of saliva: Normal composition, flow, and function. *The Journal of Prosthetic Dentistry, 85*, 162–169.

Hyun, K., Kim, S. H., Ahn, K. H., & Lee, S. J. (2002). Large amplitude oscillatory shear as a way to classify the complex fluids. *Journal of Non-newtonian Fluid Mechanics, 107*, 51–65.
Japper-Jaafar, A., Escudier, M. P., & Poole, R. J. (2009). Turbulent pipe flow of a drag-reducing rigid "rod-like" polymer solution. *Journal of Non-newtonian Fluid Mechanics, 161*, 86–93.
Jehmlich, N., Dinh, K. H. D., Gesell-Salazar, M., Hammer, E., Steil, L., Dhople, V. M., Schurmann, C., Holtfreter, B., Kocher, T., & Völker, U. (2013). Quantitative analysis of the intra- and inter-subject variability of the whole salivary proteome. *Journal of Periodontal Research, 48*, 392–403.
Joubert, M., Septier, C., Brignot, H., Salles, C., Panouille, M., Feron, G., & Tournier, C. (2017). Chewing breads: Impact on alpha-amylase secretion and oral digestion. *Food & Function, 8*, 607–614.
Kejriwal, S., Bhandary, R., Thomas, B., & Kumari, S. (2014). Estimation of levels of salivary mucin, amylase and total protein in gingivitis and chronic periodontitis patients. *Journal of Clinical and Diagnostic Research : Journal of Clinical and Diagnostic Research, 8*, ZC56–ZC60.
Kesimer, M., & Sheehan, J. K. (2008). Analyzing the functions of large glycoconjugates through the dissipative properties of their absorbed layers using the gel-forming mucin MUC5B as an example. *Glycobiology, 18*, 463–472.
Kheirandish, S., Guybaidullin, I., Wohlleben, W., & Willenbacher, N. (2008). Shear and elongational flow behavior of acrylic thickener solutions. *Rheologica Acta, 47*, 999.
Krop, E. M., Hetherington, M. M., Holmes, M., Miquel, S., & Sarkar, A. (2019). On relating rheology and oral tribology to sensory properties in hydrogels. *Food Hydrocolloids, 88*, 101–113.
Krop, E. M., Hetherington, M. M., Miquel, S., & Sarkar, A. (2020). Oral processing of hydrogels: Influence of food material properties versus individuals' eating capability. *Journal of Texture Studies, 51*, 144–153.
Lafforgue, O., Seyssiecq, I., Poncet, S., & Favier, J. (2018). Rheological properties of synthetic mucus for airway clearance. *Journal of Biomedical Materials Research Part A, 106*, 386–396.
Larson, R. G. (1999). *The structure and rheology of complex fluids*. New York: Oxford University Press.
Lecacheux, D., Mustiere, Y., Panaras, R., & Brigand, G. (1986). Molecular weight of scleroglucan and other extracellular microbial polysaccharides by size-exclusion chromatography and low angle laser light scattering. *Carbohydrate Polymers, 6*, 477–492.
Liamas, E., Connell, S. D., Ramakrishna, S. N., & Sarkar, A. (2020). Probing the frictional properties of soft materials at the nanoscale. *Nanoscale, 12*, 2292–2308.
Li, X., Lu, Y., Adams, G. G., Zobel, H., Ballance, S., Wolf, B., & Harding, S. E. (2020). Characterisation of the molecular properties of scleroglucan as an alternative rigid rod molecule to xanthan gum for oropharyngeal dysphagia. *Food Hydrocolloids, 101*, 105446.
Lopes Da Silva, J. A., Gonçalves, M. P., & Rao, M. A. (1993). Viscoelastic behaviour of mixtures of locust bean gum and pectin dispersions. *Journal of Food Engineering, 18*, 211–228.
Macakova, L., Yakubov, G. E., Plunkett, M. A., & Stokes, J. R. (2010). Influence of ionic strength changes on the structure of pre-adsorbed salivary films. *A response of a natural multi-component layer, 77*, 31–39.
Macakova, L., Yakubov, G. E., Plunkett, M. A., & Stokes, J. R. (2011). *Influence of ionic strength on the tribological properties of pre-adsorbed salivary films* (Vol. 44, pp. 956–962).
Madsen, J. B., Pakkanen, K. I., & Lee, S. (2014). Thermostability of bovine submaxillary mucin (BSM) in bulk solution and at a sliding interface. *Journal of Colloid and Interface Science, 424*, 113–119.
Manrique, Y. J., Lee, D. J., Islam, F., Nissen, L. M., Cichero, J. A. Y., Stokes, J. R., & Steadman, K. J. (2014). Crushed tablets: Does the administration of food vehicles and thickened fluids to aid medication swallowing alter drug release? *Journal of Pharmacy & Pharmaceutical Sciences, 17*, 207–219.
Manrique, Y. J., Sparkes, A. M., Cichero, J. A. Y., Stokes, J. R., Nissen, L. M., & Steadman, K. J. (2016). Oral medication delivery in impaired swallowing: Thickening liquid medications for safe swallowing alters dissolution characteristics. *Drug Development and Industrial Pharmacy, 42*, 1537–1544.
McKinley, G. H. (2005). Visco-elasto-capillary Thinning and Break-up of Complex Fluids. *The British Society of Rheology: Aberystwyth, U.K.*, 1–48.
Mckinley, G. H., & Sridhar, T. (2002). FILAMENT-STRETCHING rheometry OF complex fluids. *Annual Review of Fluid Mechanics, 34*, 375–415.
Moresi, M., Lo Presti, S., & Mancini, M. (2001). Rheology of scleroglucan dispersions. *Journal of Food Engineering, 50*, 235–245.
Newman, R., Vilardell, N., Clavé, P., & Speyer, R. (2016). Effect of bolus viscosity on the safety and efficacy of swallowing and the kinematics of the swallow response in patients with oropharyngeal dysphagia: White paper by the European society for swallowing disorders (ESSD). *Dysphagia, 31*, 232–249.
Phillips, G. O., & Williams, P. A. (2009). *Handbook of hydrocolloids*. Cambridge, UK: Woodhead Publishing Limited.
Pradal, C., & Stokes, J. R. (2016). Oral tribology: Bridging the gap between physical measurements and sensory experience. *Current Opinion in Food Science, 9*, 34–41.
Pradal, C., Yakubov, G. E., Williams, M. A. K., Mcguckin, M. A., & Stokes, J. R. (2019). Responsive polysaccharide-grafted surfaces for biotribological applications. *Biotribology, 18*, 100092.
Preininger, M. (2016). Interactions of flavor components in foods. In A. G. Gaonkar, & A. Mcpherson (Eds.), *Ingredient interactions: Effects on food quality* (2 ed.). Boca Raton: CRC press.
Pu, D., Duan, W., Huang, Y., Zhang, L., Zhang, Y., Sun, B., Ren, F., Zhang, H., & Tang, Y. (2021). Characterization of the dynamic texture perception and the impact factors on the bolus texture changes during oral processing. *Food Chemistry, 339*, 128078.
Punyadeera, C., Nouwens, A. S., Stokes, J. R., Yakubov, G., & Cooper-White, J. (2010). *Elucidation of changes in human saliva protein profiles during resting and stimulated states*. Sydney, Australia: Human Proteome World Congress (HUPO 2010).
Qazi, W. M., Johan, W., Annika, A., Olle, E., & Mats, S. (2017). Shear and extensional rheology of commercial thickeners used for dysphagia management. *Journal of Texture Studies, 48*, 507–517.
Raynal, B. D. E., Hardingham, T. E., Thornton, D. J., & Sheehan, J. K. (2002). Concentrated solutions of salivary MUC5B mucin do not replicate the gel-forming properties of saliva. *Biochemical Journal, 362*, 289–296.
Ren, Y., Yakubov, G. E., Linter, B. R., Macnaughtan, W., & Foster, T. J. (2020). Temperature fractionation, physicochemical and rheological analysis of psyllium seed husk heteroxylan. *Food Hydrocolloids, 104*, 105737.
Rodrigues, T., Galindo-Rosales, F. J., & Campo-Deaño, L. (2020). Critical overlap concentration and intrinsic viscosity data of xanthan gum aqueous solutions in dimethyl sulfoxide. *Data in Brief, 33*, 106431, 106431.
Rodrigues, S. A., Pradal, C., Yu, L., Steadman, K. J., Stokes, J. R., & Yakubov, G. E. (2021). Creating polysaccharide-protein complexes to control aqueous lubrication. *Food Hydrocolloids, 119*, 106826.
Rossetti, D., Bongaerts, J. H. H., Wantling, E., Stokes, J. R., & Williamson, A. M. (2009). Astringency of tea catechins: More than an oral lubrication tactile percept. *Food Hydrocolloids, 23*, 1984–1992.
Sarkar, A., Andablo-Reyes, E., Bryant, M., Dowson, D., & Neville, A. (2019a). Lubrication of soft oral surfaces. *Current Opinion in Colloid & Interface Science, 39*, 61–75.
Sarkar, A., Goh, K., & Singh, H. (2009). *Colloidal stability and interactions of milk-protein-stabilized emulsions in an artificial saliva*.
Sarkar, A., & Krop, E. M. (2019). Marrying oral tribology to sensory perception: A systematic review. *Current Opinion in Food Science, 27*, 64–73.
Sarkar, A., Soltanahmadi, S., Chen, J., & Stokes, J. R. (2021). Oral tribology: Providing insight into oral processing of food colloids. *Food Hydrocolloids, 117*, 106635.
Sarkar, A., Xu, F., & Lee, S. (2019b). Human saliva and model saliva at bulk to adsorbed phases - similarities and differences. *Advances in Colloid and Interface Science, 273*.
Sarkar, A., Xu, F., & Lee, S. (2019c). Human saliva and model saliva at bulk to adsorbed phases – similarities and differences. *Advances in Colloid and Interface Science, 273*, 102034.
Selway, N., Chan, V., & Stokes, J. R. (2017). Influence of fluid viscosity and wetting on multiscale viscoelastic lubrication in soft tribological contacts. *Soft Matter, 13*, 1702–1715.
Shewan, H. M., Pradal, C., & Stokes, J. R. (2020). Tribology and its growing use toward the study of food oral processing and sensory perception. *Journal of Texture Studies, 51*, 7–22.
Shewan, H. M., Stokes, J. R., & Smyth, H. E. (2020). Influence of particle modulus (softness) and matrix rheology on the sensory experience of 'grittiness' and 'smoothness. *Food Hydrocolloids, 103*.
Song, K. W., Kim, Y. S., & Chang, G. S. (2006). Rheology of concentrated xanthan gum solutions: Steady shear flow behavior. *Fibers and Polymers, 7*, 129–138.
Song, K. W., Kuk, H. Y., & Chang, G. S. (2006). Rheology of concentrated xanthan gum solutions: Oscillatory shear flow behavior. *Korea-Australia Rheology Journal, 18*, 67–81.
Sousa, P. C., Pinho, F. T., Oliveira, M. S. N., & Alves, M. A. (2011). Extensional flow of blood analog solutions in microfluidic devices. *Biomicrofluidics, 5*, Article 014108.
Stachowiak, G. W., & Batchelor, A. W. (2013). *Engineering tribology*. Butterworth-Heinemann.
Stelter, M., Brenn, G., Yarin, A. L., Singh, R. P., & Durst, F. (2002). Investigation of the elongational behavior of polymer solutions by means of an elongational rheometer. *Journal of Rheology, 46*, 507–527.
Stewart, W. E., & Sorensen, J. P. (1972). Hydrodynamic interaction effects in rigid dumbbell suspensions. II. Computations for steady shear flow. *Transactions of the Society of Rheology, 16*, 1–13.
Stokes, J. R. (2012a). 'Oral' rheology. In L. E. Jianshe Chen (Ed.), *Food oral processing: Fundamentals of eating and sensory perception*. WILEY-BLACKWELL.
Stokes, J. R. (2012b). 'Oral' tribology. In L. E. Jianshe Chen (Ed.), *Food oral processing: Fundamentals of eating and sensory perception*. WILEY-BLACKWELL.
Stokes, J. R., Boehm, M. W., & Baier, S. K. (2013). Oral processing, texture and mouthfeel: From rheology to tribology and beyond. *Current Opinion in Colloid & Interface Science, 18*, 349–359.
Stokes, J. R., & Davies, G. A. (2007a). Viscoelasticity of human whole saliva collected after acid and mechanical stimulation. *Biorheology, 44*, 141–160.
Stokes, J. R., & Davies, G. A. (2007b). Viscoelasticity of human whole saliva collected after acid and mechanical stimulation. *Biorheology, 44*, 141–160.
Stokes, J. R., & Frith, W. J. (2008). Rheology of gelling and yielding soft matter systems. *Soft Matter, 4*, 1133–1140.
Stokes, J. R., Graham, L. J. W., Lawson, N. J., & Boger, D. V. (2001). Swirling flow of viscoelastic fluids. Part 2. Elastic effects. *Journal of Fluid Mechanics, 429*, 117–153.
Stokes, J. R., Macakova, L., Chojnicka-Paszun, A., De Kruif, C. G., & De Jongh, H. H. J. (2011). Lubrication, adsorption, and rheology of aqueous polysaccharide solutions. *Langmuir, 27*, 3474–3484.
Stribiţcaia, E., Evans, C. E. L., Gibbons, C., Blundell, J., & Sarkar, A. (2020). Food texture influences on satiety: Systematic review and meta-analysis. *Scientific Reports, 10*, 12929.
Stribitcaia, E., Krop, E. M., Lewin, R., Holmes, M., & Sarkar, A. (2020). Tribology and rheology of bead-layered hydrogels: Influence of bead size on sensory perception. *Food Hydrocolloids, 104*.
Turcanu, M., Tascon, L. F., Balan, C., & Gallegos, C. (2015). In *Capillary breakup extensional properties of whole human saliva. 2015 9th international symposium on advanced topics in electrical engineering*. ATEE, 7-9 May 2015.

Veeregowda, D. H., Busscher, H. J., Vissink, A., Jager, D.-J., Sharma, P. K., & Van Der Mei, H. C. (2012). Role of structure and glycosylation of adsorbed protein films in biolubrication. *PLoS One, 7*, Article e42600.

Vinogradova, O. I., & Yakubov, G. E. (2006). Surface roughness and hydrodynamic boundary conditions. *Physical Review, 73*.

Wei, B., Romero-Zerón, L., & Rodrigue, D. (2014). Mechanical properties and flow behavior of polymers for enhanced oil recovery. *Journal of Macromolecular Science, Part B, 53*, 625–644.

Witt, T., & Stokes, J. R. (2015). Physics of food structure breakdown and bolus formation during oral processing of hard and soft solids. *Current Opinion in Food Science, 3*, 110–117.

Xu, Y., & Stokes, J. R. (2020). Soft lubrication of model shear-thinning fluids. *Tribology International, 152*, 106541.

Yakubov, G. E. (2014). Lubrication. In A. J. M. Ligtenberg, & E. C. I. Veerman (Eds.), *Saliva: Secretion and functions*.

Yakubov, G. E., Gibbins, H., Proctor, G. B., & Carpenter, G. H. (2014). *Oral mucosa: Physiological and physicochemical aspects. Mucoadhesive materials and drug delivery systems*.

Yakubov, G. E., Macakova, L., Wilson, S., Windust, J. H. C., & Stokes, J. R. (2015). Aqueous lubrication by fractionated salivary proteins: Synergistic interaction of mucin polymer brush with low molecular weight macromolecules. *Tribology International, 89*, 34–45.

Yakubov, G. E., Mccoll, J., Bongaerts, J. H. H., & Ramsden, J. J. (2009). Viscous boundary lubrication of hydrophobic surfaces by mucin. *Langmuir, 25*, 2313–2321.

Yanaki, T., & Norisuye, T. (1983). Triple helix and random coil of scleroglucan in dilute solution. *Polymer Journal, 15*, 389.

Zirnsak, M. A., Boger, D. V., & Tirtaatmadja, V. (1999). Steady shear and dynamic rheological properties of xanthan gum solutions in viscous solvents. *Journal of Rheology, 43*, 627–650.